AGU ADVANCING EARTH AND SPACE SCIENCE

Water Resources Research

RESEARCH ARTICLE
10.1029/2021WR030957

Potential Satellite Monitoring of Surface Organic Soil Properties in Arctic Tundra From SMAP

Yonghong Yi[1,2,3], Richard H. Chen[3], John S. Kimball[4], Mahta Moghaddam[5], Xiaolan Xu[2], Eugénie S. Euskirchen[6], Narendra Das[7], and Charles E. Miller[3]

[1]Joint Institute for Regional Earth System Science and Engineering, University of California, Los Angeles, Los Angeles, CA, USA, [2]Now at College of Surveying and Geo-Informatics, Tongji University, Shanghai, China, [3]Jet Propulsion Laboratory, California Institute of Technology, Los Angeles, CA, USA, [4]Numerical Terradynamic Simulation Group, The University of Montana, Missoula, MT, USA, [5]Department of Electrical Engineering, University of Southern California, Los Angeles, CA, USA, [6]Institute of Arctic Biology, University of Alaska Fairbanks, Fairbanks, AK, USA, [7]Department of Biosystems and Agricultural Engineering, Michigan State University, East Lansing, MI, USA

Key Points:

- Tundra soil with higher organic carbon concentration or low bulk density shows more rapid soil drydown process
- Accounting for effects of soil carbon decomposition state on soil hydraulic properties is important to model tundra soil moisture dynamics
- L-band data are sensitive to tundra soil moisture and carbon properties with potential to improve modeling of active layer thaw dynamics

Supporting Information:

Supporting Information may be found in the online version of this article.

Correspondence to:

Y. Yi,
yonghong_yi@tongji.edu.cn

Citation:

Yi, Y., Chen, R. H., Kimball, J. S., Moghaddam, M., Xu, X., Euskirchen, E. S., et al. (2022). Potential satellite monitoring of surface organic soil properties in Arctic tundra from SMAP. *Water Resources Research*, *58*, e2021WR030957. https://doi.org/10.1029/2021WR030957

Received 31 JUL 2021
Accepted 12 MAR 2022

Author Contributions:

Conceptualization: Yonghong Yi, Richard H. Chen, Charles E. Miller
Formal analysis: Yonghong Yi
Funding acquisition: Yonghong Yi, John S. Kimball, Narendra Das
Methodology: Yonghong Yi, Richard H. Chen, Mahta Moghaddam, Xiaolan Xu
Project Administration: Charles E. Miller
Resources: John S. Kimball
Software: Yonghong Yi
Validation: Yonghong Yi, Richard H. Chen, Mahta Moghaddam, Xiaolan Xu, Eugénie S. Euskirchen
Writing – original draft: Yonghong Yi
Writing – review & editing: Richard H. Chen, John S. Kimball, Mahta Moghaddam, Eugénie S. Euskirchen, Narendra Das, Charles E. Miller

Abstract Surface organic carbon content and soil moisture (SM) represent first-order controls on permafrost thaw and vulnerability, yet remain challenging to map accurately. Here we explored the links between surface organic soil properties and SM dynamics in the Alaska North Slope through data analysis and process-based modeling. Our analysis, based on in situ SM and brightness temperature data from the Soil Moisture Active Passive (SMAP) mission, indicated that the SM drydown process in Arctic tundra is closely related to surface soil organic carbon (SOC) properties. More rapid drydown was generally observed in areas with high SOC concentration (SOCC) or low bulk density. The drydown timescale derived from the SMAP polarization ratio (PR) was significantly correlated with SoilGrids surface (0–5 cm) SOCC data ($R = -0.54 \sim -0.68$, $p < 0.01$) at regional scale. To understand the process, we used a coupled permafrost hydrology and microwave emission model to simulate changes in the L-band PR during the thaw season. The model accounts for the variations in organic soil hydraulic and dielectric properties with SOC content and decomposition state. Model sensitivity runs showed larger L-band PR decreases during the early thaw season in soils with higher SOCC consistent with the above analysis, whereby highly organic soils (SOCC > 34.8%) drain water more easily with a larger amount of water discharged or lost (through evapotranspiration) relative to soils with less carbon concentration (SOCC < 17.4%). Our findings indicate that satellite L-band observations are sensitive to tundra SM and carbon properties, and may provide critical constraints on predictions of Arctic permafrost thaw and vulnerability.

1. Introduction

Permafrost underlies about 24% of the exposed land areas in the Northern Hemisphere with more than 85% of the permafrost distributed above 50°N latitude (Zhang et al., 2008). Pronounced warming has occurred in the northern high latitudes, which has induced widespread changes in the northern permafrost region, including increasing permafrost ground temperatures, active layer deepening, enhanced duration of the zero-curtain period and talik formation at depth (Biskaborn et al., 2019; Connon et al., 2018; Yi et al., 2019). Permafrost acts as a barrier to vertical water flow and exerts strong control on soil hydrologic conditions. Warming-induced permafrost thaw will trigger major changes in the Arctic hydrologic system, including alterations to soil moisture (SM) regimes, the connectivity of inland waters, streamflow seasonality, and the partitioning of water stored above and below ground (Vonk et al., 2019). This shifting soil hydrology with permafrost thaw will create a fragmented landscape composed of both drier and wetter soil conditions, which will largely determine potential climate and carbon feedbacks of boreal-Arctic ecosystems (Liljedahl et al., 2016). However, pan-Arctic characterizations of permafrost thaw and SM variations remain highly uncertain despite documented rapid changes (Andresen et al., 2020).

The northern permafrost region contains a vast amount of soil organic carbon (SOC; Hugelius et al., 2020). Highly organic soils can act as strong insulators due to their distinctly different hydraulic and thermal properties, and can modulate how permafrost thaw responds to warming (Lawrence & Slater, 2008; Yi et al., 2018). The effects of organic soil on ground temperature evolution are also strongly regulated by the soil structure and water content (Zwieback et al., 2019). However, representing such effects in global models has been challenging, partly due to a lack of effective parameterization of organic soil hydraulic properties (Decharme et al., 2016; Paquin &

Sushama, 2015). Organic soil hydraulic properties can change dramatically depending on the carbon content and decomposition state of the soil organic matter (SOM). Undecomposed (fibric) organic soils with very low density have large hydraulic conductivity and are highly permeable, while more decomposed (hemic or sapric) organic soils exhibit higher density, higher suction, and low hydraulic conductivity (Letts et al., 2000; Verry et al., 2011). The variability in soil hydraulic properties also has a large impact on the soil thermal properties by affecting water flow and retention, which influences soil heat transfer and active layer freeze/thaw (FT) processes. Previous studies have demonstrated that accounting for the variability of hydraulic properties within the organic soil profile can improve model simulated water table depth, soil temperatures, and hydrologic fluxes in the northern high latitudes (Bechtold et al., 2019; Guimberteau et al., 2018).

Although surface SOM represents one of the major controls on active layer thaw dynamics and SM variations, large uncertainties remain in current estimates of the pan-Arctic SOC stock (Hugelius et al., 2020; Mishra et al., 2021). SOC is the carbon component (~58%) of SOM, which is more measurable than other components of SOM. As a result, SOC is typically reported in regional and global soil data sets (Hugelius et al., 2020; Tifafi et al., 2018). Mishra and Riley (2015) showed that the variance of SOC content varied at different scales, but remained constant beyond the scale of ~500 m, with different environmental factors controlling the SOC spatial variability at different scales. In situ or ground-based remote sensing measurements generally fail to capture such variability. A variety of methods including geospatial analysis and machine-learning data-driven approaches have been applied to upscale in situ SOC content to provide grid-cell mean estimates of SOC for direct comparison with satellite or model-based products (e.g., Mishra et al., 2021; Mishra & Riley, 2015). However, the accuracy of the above methods is limited by available in situ SOC measurements that generally fail to capture the spatial variability of SOC across the vast northern permafrost domain.

Soil dielectric constant is primarily dependent on soil physical characteristics, the amount of water content, and soil temperature (Schmugge, 1983). Increasing soil water volume will lead to significant increases in both the real and imaginary parts of the dielectric constant of soil due to the high dielectric constant of water. The soil dielectric constant dependence on soil type (or texture) reflects the varying amount of soil water bound to the particle surfaces in different soils. The presence of SOM can modify the soil composition, including the percentage of free-water and bound-water components, and in turn affect the dielectric constant. Microwave remote sensing, especially from longer wavelengths such as L-band, can capture significant dielectric changes resulting from soil FT transitions or drying/wetting events (Chan et al., 2016; Derksen et al., 2017; Kerr et al., 2012), and may also provide other useful information on SOM composition and soil water storage. Previous studies have reported strong L-band sensitivity to surface SM in both tundra and boreal forest, with the sensing depth varying from ~1 cm to tens of centimeters depending on surface SM conditions (Colliander et al., 2020; Escorihuela et al., 2010; Gherboudj et al., 2012). Since the capacity of this soil layer to hold and conduct water varies with soil type, the differences in microwave emissivity over time should indicate the differences in the soil hydraulic properties. A few studies have demonstrated a strong qualitative relationship between L-band brightness temperature and soil type and properties (e.g., saturated hydraulic conductivity; Burke et al., 1998; Camillo et al., 1986; Mattikalli et al., 1998). A follow-on study has successfully inverted meaningful hydraulic parameters using SM retrievals from L-band brightness temperature (Santanello et al., 2007). However, very few studies have discussed the potential of L-band brightness temperature to provide reliable estimates of surface soil composition (including SOC) and moisture conditions in organic-rich soils or peatlands across the northern permafrost region (Bechtold et al., 2020; Jonard et al., 2018).

Our goal in this study was to test the feasibility of an integrated process model—remote sensing solution to potentially provide reliable, regional-scale SM and SOC estimates over the vast pan-Arctic region. Our model accounts for variability in the organic soil hydraulic and dielectric properties in the soil parameterization that is generic to facilitate model extrapolations over the entire pan-Arctic region. Furthermore, we combined data analysis with model simulations to study the linkage between tundra SM dynamics (particularly the soil drydown characteristics) and organic soil properties on the Alaska North Slope. The shape of SM drydown, which is generally defined as the SM time series directly following a precipitation event with zero infiltration input, is determined by multiple processes including drainage, runoff and evapotranspiration (McColl et al., 2017). The rate at which soil drydown occurs, is a measure of SM "memory," important for studying land surface and atmosphere feedbacks (McColl et al., 2019). In this study, we first derived the soil drydown characteristics using in situ SM data and SMAP (Soil Moisture Active Passive) satellite L-band (1.41 GHz) polarization ratio (PR) observations. We then

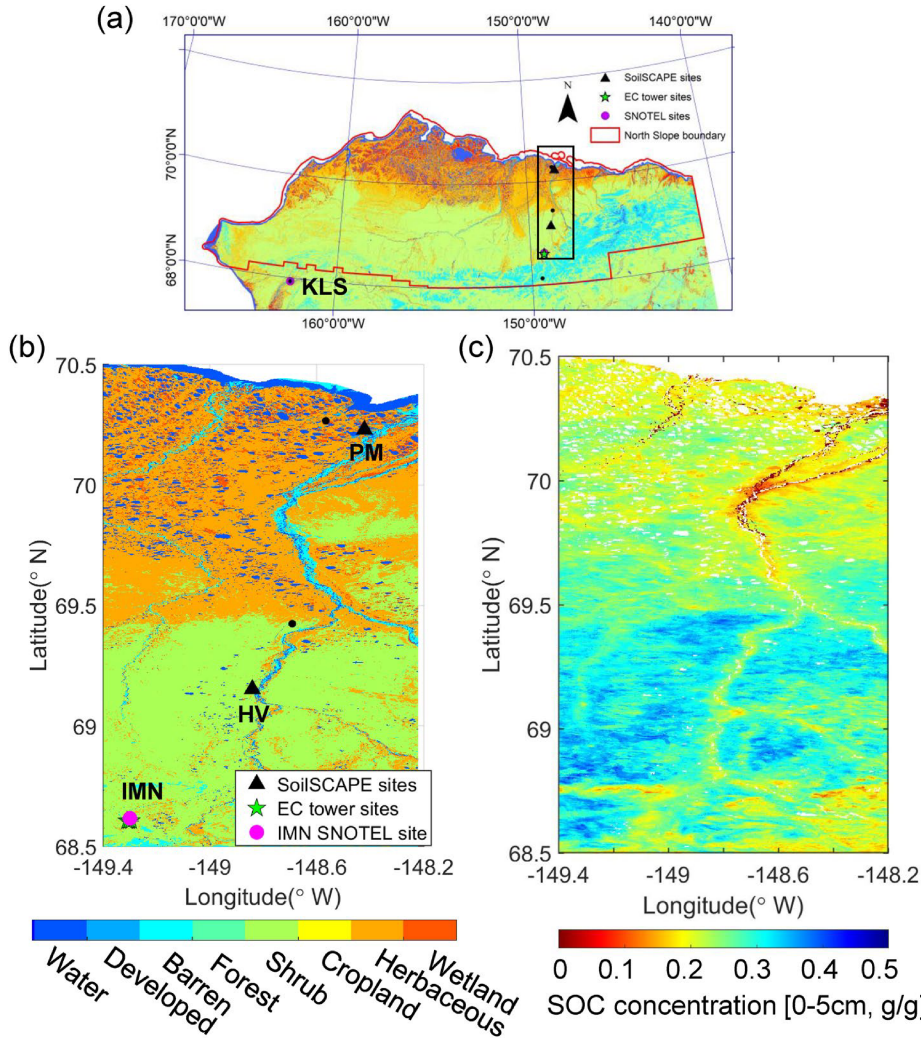

Figure 1. Study area (a) and location of in situ sites. A subregion (approximate location indicated by the black box in a) along the Deadhorse Highway (DHN, (b) was selected for the regional analysis on soil drydown process. Both panel (a) and (b) are based on the NLCD land cover map, with the legend shown in panel (b). Additional SNOTEL sites in the North Slope are shown as black dots, which were used to evaluate the Daymet precipitation data (Thornton et al., 2020). The surface SOC concentration derived from the SoilGrids version1 data set for the DHN subregion is shown in panel (c).

examined the PR and SM sensitivity to soil carbon properties indicated from a regional SOC data set (SoilGrids). Finally, we used a coupled permafrost hydrology and microwave emission model to clarify the sensitivity of the L-band PR to tundra SM changes and surface organic soil properties.

2. Study Area and Data Analysis

2.1. Study Area and In Situ Data

Our study area is located on the Alaska North Slope (≥~68°N, Figure 1), which encompass the Beaufort Coastal Plain and Brooks Foothills ecoregions (Berner et al., 2018). Based on the 30-m National Land Cover Database (NLCD, Jin et al., 2013), this area is dominated by two major tundra types, including Sedge/Herbaceous and Scrub/shrub tundra. The Beaufort Coastal Plain supports extensive lowland tundra plant communities, dominated by sedges and small shrubs. The warmer Brooks Foothills supports tussock tundra, shrub tundra, and mixed tundra communities. This area is underlain by continuous permafrost, which prevents soil drainage and promotes waterlogged soils and wetland vegetation representative of the larger tundra biome.

Table 1
The List of In Situ Sites and Data Used in This Study

	Coordinates	Data sets	Period	Note
EC tower sites at Imnavait Creek watershed	US-ICh: 68°36′24″N, 149°17′45″W US-ICs: 68°36′21″N, 149°18′40″W US-ICt: 68°36′23″N, 149°18′15″W	Latent heat fluxes, surface (5 cm) and deep T_{soil} and SM, wind speed	2008–2020	Deep T_{soil} and SM available from the neighboring borehole site; data used for hydrology model calibration and validation
Imnavait Creek (IMN) SNOTEL site	68°37′N 149°18′W	Surface (~5 cm) SM, T_{soil} precipitation	2012–2020	Soil drydown analysis; model calibration and validation
Kelly Station (KLS) SNOTEL site	67°56′N 162°17′W	Surface (~5 cm) SM, T_{soil}, Precipitation	2015–2020	Soil drydown analysis
Prudhoe Meadow (PM) SoilSCAPE site (node S5)	70°13′47″N 148°25′19″	Surface (~5 cm) SM, T_{soil}	2016–2018	Soil drydown analysis; no data after August 2018
Happy Valley (HV) SoilSCPAE site (node S1)	69°9′11″N 148°50′31″W	Surface (~5 cm) SM, T_{soil}	2016–2017; 2019–2020	Soil drydown analysis; gaps between 2017 and 2019

We used surface (~5 cm depth) SM data from two SNOTEL (SNOwpack TELemetry, http://www.wcc.nrs.usda.gov) sites and two Soil moisture Sensing Controller and oPtimal Estimator (SoilSCAPE) sites (http://soilscape.usc.edu) for the soil drydown analysis (Table 1). There are four SNOTEL sites located within the North Slope Borough boundary (Figure 1a); however, we only chose the Imnavait Creek (IMN) site, since other sites either have no SM measurements, or are located in the barren mountain area. In addition, we also included the Kelly Station (KLS) SNOTEL site adjacent to the North Slope region in our analysis. This site was classified as "scrub/shrub" tundra by the NLCD map, though this area may have some tree canopy coverage based on the site characterization data (Figure S1 in Supporting Information S1). The four sites create a north-south transect from the Arctic Coastal Plain to the Brooks Range foothills. Half-hourly soil dielectric constant data were available since August 2016 at the SoilSCAPE sites. We converted the dielectric data to SM using the soil dielectric model described in Appendix A, and SOM measurements at the two sites as inputs to the dielectric model. The SOM content is ~22 ± 5% at the topsoil (depth of ~15 cm) for the PM site, and ~90 ± 4% at surface (depth of ~7 cm) for the HV site (Bakian-Dogaheh et al., 2020). The underlying mineral soil texture is silt loam at the PM site, and silty clay loam for the HV site. Varying SOM content by 10% leads to less than 5% cm^3/cm^3 variations in the model estimated SM. A soil dielectric model tailored for organic soil is under development using field soil samples and laboratory measurements, which shall provide more accurate SM estimates. Multiple nodes were installed at each SoilSCAPE site, although the data temporal coverage is much lower compared with the SNOTEL sites.

For the hydrology model calibration and validation, we mainly used the data from three Eddy Covariance (EC) tower sites within the Imnavait Creek watershed (Table 1), including dry heath, moist acidic tussock, and wet sedge (Fen) tundra (Euskirchen, Bret-Harte, et al., 2017). Mean annual air temperature and precipitation at this site are −7.4°C and 324 mm, respectively. The surface soil organic layer varies from 34 ± 2.4 cm in wet sedge tundra to 15 ± 1.4 cm in the tussock tundra and 2.3 ± 0.3 cm in the dry heath tundra. Surface (~5 cm depth) soil temperature and moisture were available at the three tower sites; deep soil temperature (T_{soil} at 34, 50, and 90 cm depths) and SM (14, 39, and 53 cm) are available from a neighboring borehole site (Euskirchen, Bret-Harte, et al., 2017). Surface SM at the tower sites have large uncertainties including abrupt changes in the SM measurements at the Tussock tundra site; therefore, we also used surface soil moisture and temperature data from the adjacent Imnavait Creek SNOTEL site for model calibration and validation, which is located in areas with surface conditions more similar to the dry heath tundra site according to the tower PI (Euskirchen).

2.2. Soil Moisture Drydown Analysis

The soil drydown process can be modeled using an exponential decay function (Shellito et al., 2016):

$$\theta(t) = Ae^{(-t/\tau_0)} + \theta_f \quad (1)$$

where θ is the surface SM (cm^3/cm^3), and t is the time since the beginning of the drydown (days). A, τ_0, and θ_f are empirical fitting parameters describing the magnitude of SM drying (cm^3/cm^3), the drydown timescale (days), and the residual SM (cm^3/cm^3), respectively. The parameter τ_0 is of particular interest as a measure of the SM "memory," and global studies have shown large variability in τ_0 with climate regime, soil texture, measurement depth, etc. (Kurc & Small, 2004; McColl et al., 2017; Rondinelli et al., 2015; Shellito et al., 2016). However, none of the studies have particularly looked into how this parameter varies in the Arctic region.

We used both the in situ SM (Table 1) and SMAP brightness temperature data to study the SM drydown process in Arctic tundra. Soil thawing and freezing can lead to changes in the liquid soil water content. Therefore, we first used the air temperature data to define the surface thaw and freeze onset, and mask out frozen and freeze/thaw transitional periods. The freeze (thaw) onset was defined as the date when both the air temperature at that day and the 7-day moving average drop below (rise above) 0°C. We then identified individual drydown periods, with significant (>∼8 mm) rainfall occurring prior to the drydown period, and with less than 2 mm precipitation occurring during the drydown period. Besides precipitation inputs, soil wetting can also be associated with soil thawing in the permafrost area (Figure 2). Therefore, we also extracted the apparent soil "drydown" events that occurred within the 30-day period after the thaw onset, even though there may be low precipitation accumulation prior to the "drydown" period. During this period, the soil "drydown" process can be different from classical "drydown" events in the middle latitudes; during early thaw period in the Arctic, surface soil drainage may occur simultaneously with subsurface thawing. We chose the "30-day period" because previous studies based on in situ SM data and satellite SM retrievals have showed that the soil drydown time constant is generally less than 20 days (McColl et al., 2017; Shellito et al., 2016). In addition, the "30-day period" covers the majority of drydown periods (i.e., low precipitation input) in the study area. For the analysis, we only analyzed drydown events lasting longer than 5 days. In situ air temperature and precipitation were used for the analysis at the SNOTEL sites. For the SoilSCAPE sites, we used the Daymet surface meteorology (Thornton et al., 2020) for the analysis.

We used the Polarization Ratio (PR) derived from the 9-km SMAP L1C_TB_E Northern Hemisphere polar product (Chaubell et al., 2020) to study the soil drydown process at both site and regional scales (Figure 1b). The NASA SMAP mission was launched in January 2015 and acquires vertically (V) and horizontally (H) polarized brightness temperature (Tb) measurements at 1.4 GHz and 40° incident angle. The Tb data are acquired from the sun-synchronous polar-orbiting satellite at consistent 6 a.m./p.m. equatorial crossing times and with ∼40-km native footprint resolution. The SMAP Tb data are acquired globally with 1–3 days repeat measurements and daily coverage at the higher latitudes (>50°N/S) due to converging orbital swath acquisitions toward the poles. The Tb data are composited individually for ascending and descending orbits and mapped to 9 km grid resolution global and polar EASE-grid version 2 projections using a Backus-Gilbert spatial interpolation process in the SMAP L1C_TB_E product (Chaubell et al., 2020). We averaged the ascending and descending overpasses to derive daily mean brightness temperature.

The PR was defined as the polarization difference of the daily mean brightness temperature, normalized by the mean brightness temperature:

$$PR = \frac{T_{bv} - T_{bh}}{(T_{bh} + T_{bv})/2} \quad (2)$$

where T_{bv} and T_{bh} represent the brightness temperature at V and H pol. Our study area is mainly dominated by herbaceous and shrub tundra, with relatively low biomass. Therefore, we assume SM is one of the main factors affecting the PR values. Generally, surface soil is very wet right after spring thaw in Arctic tundra, and then gradually dries out during the thaw season without significant precipitation inputs. Figure 2 shows the time series of in situ surface SM data along with the SMAP L-band PR time series at the SNOTEL and SoilSCAPE sites. Here, the SMAP PR gradually drops during the early thaw period at the tundra sites, consistent with the in situ surface SM data. However, the L-band PR generally shows an earlier thaw onset compared with the SM data at 5-cm depth, while the surface thaw onset derived from the air temperature data corresponds well with the thaw onset indicated by the PR time series. Other than SM changes, vegetation growth and resultant changes in the vegetation water content also affect the PR values (Paloscia et al., 2018). Therefore, we limited our analysis to the first 30-day period after spring thaw onset (similar to the in situ SM analysis) to reduce the impact of vegetation water content

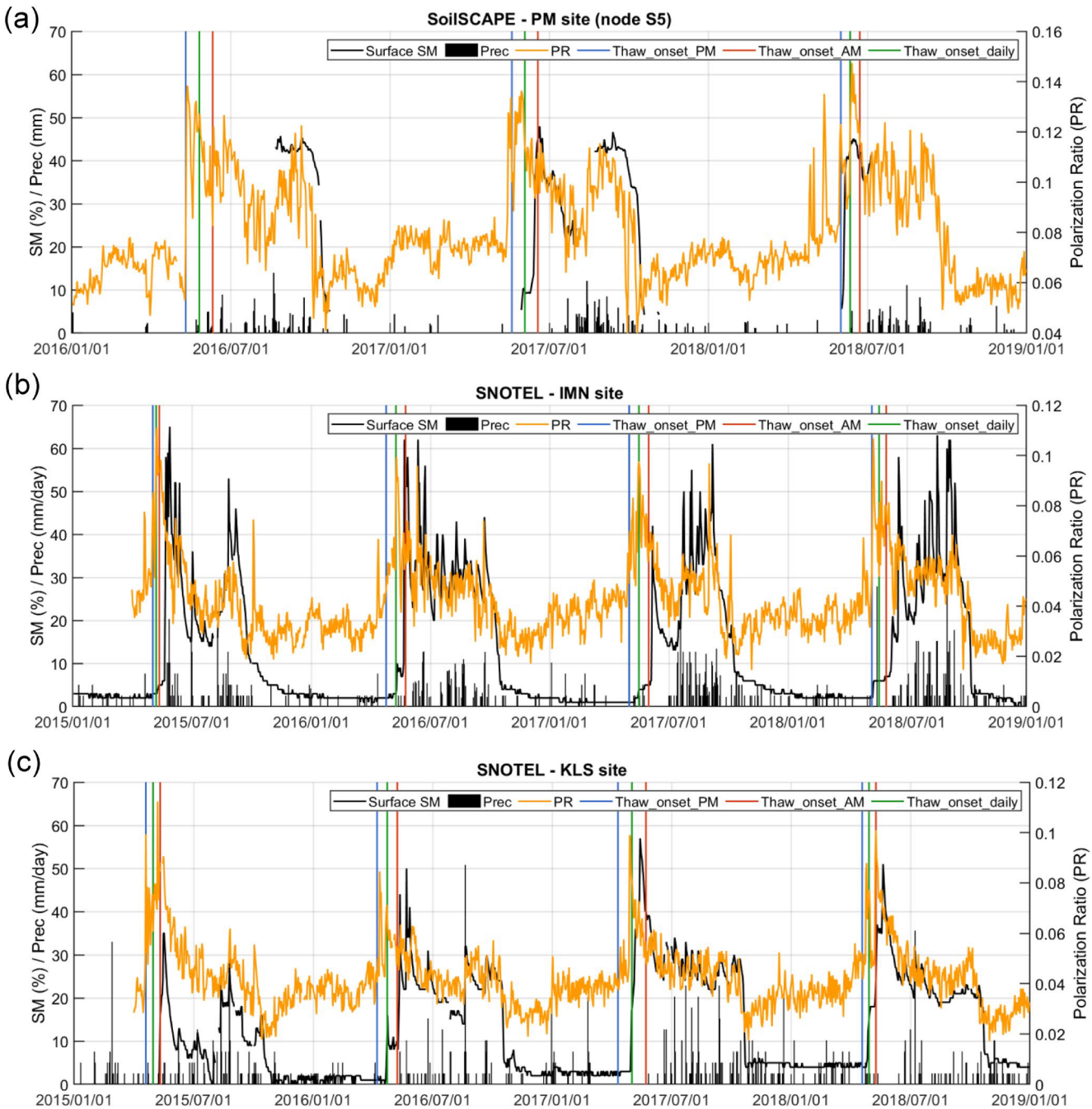

Figure 2. Daily time series of in situ SM, L-band PR derived from SMAP brightness temperature data at the SNOTEL and SoilSCAPE sites, used for the soil drydown analysis, shown with daily precipitation and thaw onset derived from daily maximum (thaw_onset_PM), minimum (thaw_onset_AM) and mean air temperature (thaw_onset_daily) data. The data at the HV SoilSCAPE site were not shown due to large data gaps and no overlap between PR and SM data during the spring thaw period.

changes on the L-band Tb and PR. The selection of drydown periods for the PR data is similar to the in situ SM drydown analysis, although no additional constraints were added to the prior accumulated precipitation amount.

We fitted the three parameters, A, τ_0, and θ_f, by minimizing the sum of squared errors between modeled SM (or PR) with in situ (or SMAP) observations. For the site scale analysis, we did not perform data fitting for each individual drydown event, but pooled all data together, due to large uncertainties in the precipitation and SM measurements. For the regional-scale analysis, we selected a subregion along the Dalton Highway (DHN) covering an area of 1.2° × 2° (Figure 1b), which encompassed all the in situ sites except for the Kelly Station SNOTEL site.

We chose this region mainly because it experienced very low precipitation during the spring thaw period in 2017 (only a few mms of rainfall were recorded during June), enabling longer drydown events to be extracted from the PR data from the overlapping SMAP observation period (2015–2020). For the analysis, we excluded all 9-km grid cells with surface open water area greater than 1% indicated by the SMAP ancillary data. SoilGrids 250 m SOC concentration (SOCC) and bulk density data (version 1: Hengl et al., 2017; version 2: Poggio et al., 2021) were used to compare with the drydown timescale derived from the SMAP PR data. The 250-m SoilGrids data were aggregated and resampled to the same 9-km Northern Hemisphere EASE-grid 2 projection as the SMAP PR data prior to the comparison. Our preliminary analysis indicates that the two SoilGrids data sets show quite different spatial pattern across the entire North Slope, but are relatively more consistent in the DHN subregion, likely because more in situ SOC data are available in this region. With more high-quality SOC and precipitation (used for identifying drydown events) data available in the future, we will be able to extend our analysis to a larger domain.

3. Model Simulations

We studied the sensitivity of the SMAP L-band PR time series to the soil drydown process during the thaw season and tried to identify the main factors controlling this sensitivity, by coupling a permafrost hydrology model with the widely used tau-omega model. The hydrology model provides soil moisture and temperature simulations that were converted to soil dielectric constant and used as primary inputs to the tau-omega model. The impact of varying SOM on soil hydraulic, thermal and dielectric properties was also represented in the model simulation as described below.

3.1. Hydrology Model Simulation

We used the pan-Arctic Water Balance Model (PWBM; Rawlins et al., 2013) with main improvements on the evapotranspiration (ET) modeling component to simulate soil thermal and hydrologic conditions in this study. The PWBM model used here is an extension of a simple large-scale pan-Arctic water balance model, but has been improved to include more detailed processes to account for organic soils, changes in snow cover properties and soil water phase change on the soil FT process (Rawlins et al., 2013; Yi et al., 2015). Other model improvements, including new parameterizations for surface fractional open water and soil carbon content (Rawlins et al., 2019), were not used here. We used a different organic soil parameterization in the PWBM for this study as discussed in Section 3.1.1. The model simulates snow/ground and subsurface temperature dynamics using a 1-D heat transfer equation, and the 1-D Richards equation was used to simulate soil water movement within the soil profile. The PWBM model defines 23 soil layers down to 60 m below surface, with a finer vertical resolution in the surface layers. The center of each layer in the top ∼1 m soil profile is located at 1, 3, 8, 13, 23, 33, 45, 55, 70, 105 cm depths. Multiple snow layers are used to account for the effects of seasonal snow cover evolution on the ground thermal regime. More model details can be found in Rawlins et al. (2013) and Yi et al. (2015).

We modified the ET scheme in the original PWBM model to improve both the model simulated ET and SM. The original PWBM model did not distinguish soil evaporation from plant transpiration, and soil water loss through ET was calculated for the entire root zone. This approach may overestimate total ET when the surface soil is dry or vegetation cover is low. In this study, we separated soil evaporation from plant transpiration. For soil evaporation, water was taken from the first 2 soil layers (∼5 cm), while for transpiration water was taken from the rooting zone or thawing depth. The details were provided in Appendix B.

3.1.1. Soil Parameterization Adapted for Organic Soil

Organic soils have distinctly different hydraulic properties from mineral soils, and should be accounted for when modeling soil conditions in the northern permafrost region. Depending on the degree of decomposition, highly organic histosol or peat soils can be classified as fibric (least decomposed), hemic (moderately decomposed), and sapric (highly decomposed; Verry et al., 2011). Fibers are fragments of plant tissue representing the undecomposed or partially decomposed portions of soil organic materials. The fiber content (FC) of SOM is a proxy measure of the degree of organic soil decomposition that affects the bulk density, porosity, and pore size distribution, and thus can have significant impact on soil water-retention characteristics and hydraulic conductivity. Chen et al. (2019) proposed a new soil parameterization that incorporates “fiber content” to describe the soil hydraulic properties, which was used in this study.

The soil bulk density can be expressed as an exponential function of soil organic matter (SOM in mass concentration, g/g; Hossain et al., 2015):

$$\rho_b = \rho_{bm} \cdot e^{(-\gamma_{OM} \cdot \mathrm{SOM})} \tag{3}$$

where ρ_{bm} is the bulk density (g/cm^3) of pure mineral soil (i.e., SOM = 0), and γ_{OM} is the exponential decay rate. FC can be related to soil bulk density using an exponential function based on data fitting using the soil database collected by the US Department of Agriculture-National Cooperative Soil Survey (Chen et al., 2019):

$$FC = 0.9887 \cdot e^{-5.512\rho_b} \tag{4}$$

This equation gives a similar estimate of FC as the quadratic function proposed from previous studies (Boelter, 1969; Verry et al., 2011) for soils with low bulk density $\rho_b < 0.3$ g/cm^3; however, here we used the above equation to cover the full range of ρ_b. Instead of dividing soil solids into just mineral and organic materials as most land surface models do, we incorporated FC into the parameterization and considered three solid components: mineral (m), humus (h), and fibrous (f) materials. The humus and fibrous materials represent the portions of organic matter that are well-decomposed and slightly decomposed with different FC values, respectively. Their volumetric fractions (v_f, v_h, v_m, with $v_f + v_h + v_m = 1 - \varnothing$) can be determined using the organic mass concentration and FC:

$$\begin{aligned} v_f &= \frac{\rho_b}{\rho_f} \times \mathrm{SOM} \times \mathrm{FC} \\ v_h &= \frac{\rho_b}{\rho_h} \times \mathrm{SOM} \times (1 - \mathrm{FC}) \\ v_m &= \frac{\rho_b}{\rho_m} \times (1 - \mathrm{SOM}) \end{aligned} \tag{5}$$

where $\varnothing$ is the soil porosity (cm^3/cm^3), ρ_m, ρ_h, and ρ_f define the specific densities for mineral, hemic/sapric, and fibric soil materials and are 2.65 g/cm^3, 1.80 g/cm^3, 0.60 g/cm^3, respectively. Their subphase fractions within the soil solids (f_{v_f}, f_{v_h}, f_{v_m}, with $f_{v_f} + f_{v_h} + f_{v_m} = 1$) can be expressed as:

$$\begin{aligned} f_{v_f} &= v_f/(1 - \varnothing) \\ f_{v_h} &= v_h/(1 - \varnothing) \\ f_{v_m} &= v_m/(1 - \varnothing) \end{aligned} \tag{6}$$

The PWBM model uses the Campbell function (Campbell, 1974) to relate soil matric potential and hydraulic conductivity to volumetric SM using an empirical parameter b. Besides the Campbell shape parameter b, the key parameters affecting soil water transfer also include the porosity, air-entry potential (ψ_s), and saturated hydraulic conductivity (k_s), which can vary substantially depending on the organic matter content and FC. We therefore applied a weighted combination approach using the sub-phase fractions, and the parameter values (X) that are representative for each principle solid component (i.e., X_m, X_h, X_f). The literature values of the above hydraulic parameters reported for fibric, hemic, and sapric peat (e.g., Letts et al., 2000; Verry et al., 2011) represent values for soil mixtures of humus and fibrous materials. We assumed those values corresponding to soils with SOM concentrations of 100% and 35–45%, respectively in this study. We then used the hydraulic parameters of fibric and hemic/sapric peat and their subphase volumetric fraction (Equation 6) to solve for the nominal values of purely "humus" and "fibrous" materials (i.e., X_h, X_f). Then, the hydraulic parameters for any soil mixture can be calculated as the weighted average of the nominal values of principal solid components as described below.

For the soil water-retention curve, there are two parameters to be determined: the air-entry potential ψ_s and the exponent b. The values of ψ_s show a very weak dependence on degree of decomposition (Letts et al., 2000). We thus assumed a linear transition from fibric peat (SOM = 1) to sapric peat (SOM_1 = 35–45%), followed by a quadratic transition from sapric peat to purely mineral soil:

$$\psi_s = \psi_{s,s} + \frac{(\mathrm{SOM} - SOM\_1)}{1 - SOM\_1}(\psi_{s,f} - \psi_{s,s}) \quad \text{if SOM} \geq SOM\_1$$

$$\psi_s = \psi_{s,s} + \frac{(\mathrm{SOM} - SOM\_1)^2}{SOM\_1^2}(\psi_{s,m} - \psi_{s,s}) \quad \text{if SOM} \le SOM\_1 \tag{7}$$

where $\psi_{s,s}$ and $\psi_{s,f}$ are the air-entry potential (cm) for fibric and sapric peat, respectively. For the pure mineral soil, $\psi_{s,m} = -10^{(1.88-0.0131\times sand\%)}$. For the exponent b, we use the weighted arithmetic mean to calculate b for mixed soils:

$$b = f_{v\_f} \times b_f + f_{v\_h} \times b_h + f_{v\_m} \times b_m \tag{8}$$

where b_f, b_h, b_m are the values for pure fibrous, humus, and mineral materials, respectively, with $b_m = 2.91 + 0.159 \times clay\%$. The values of b_f and b_h can be solved based on the b values of fibric (SOM = 1) and sapric peat (SOM = SOM_1), given their sub-phase fractions of the three soil constituents. For saturated hydraulic conductivity, we used the weighted arithmetic mean of $log_{10}k_s$:

$$log_{10}k_s = f_{v\_m} log_{10}k_{s,m} + f_{v\_h} log_{10}k_{s,h} + f_{v\_f} log_{10}k_{s,f} \tag{9}$$

where $k_{s,f}$, $k_{s,h}$ and $k_{s,m}$ are the saturated hydraulic conductivity (m/s) for the fibrous, humus, and mineral materials, with $k_{s,m} = 7.0556 \cdot 10^{-6.884+0.0153\times sand\%}$. Similar as above, the values of $k_{s,f}$ and $k_{s,h}$ can be solved based on the K_s values of fibric and sapric peat.

Table S1 in Supporting Information S1 provides the parameter values for fibric and hemic/sapric peat that were used to solve the nominal value of pure fibrous and humus soil materials used in this study. The hydraulic parameters of soils with varying SOM values and mineral soil texture of sand = 44% and clay = 25% are plotted in Figure 3, showing that the above parametrization is able to capture the slow drainage or water flows in well-decomposed organic soils. The relationship between soil porosity and soil bulk density (or SOM) was also consistent with data presented in O'Connor et al. (2020) and data collected from our recent field work in the study area (Bakian-Dogaheh et al., 2020; Figure S2 in Supporting Information S1).

3.2. Tb Simulation

We used the established tau-omega model to simulate the L-band brightness temperature and polarization ratio. The basic concept and description of the tau-omega model can be found in a number of studies (e.g., Kerr et al., 2012; Wigneron et al., 2008), and we mainly describe the model parameterization here. The main parameters in the tau-omega model include the vegetation optical depth (VOD, τ_p), soil roughness parameter (h), and single-scattering albedo (ω_p), where the subscript p refers to polarization (V or H). Under low to moderate vegetation cover, the single-scattering albedo is very low and we used 0.05 in this study. The VOD was found to be linearly related to the vegetation water content (VWC) using the b_f parameter through $\tau_p = b_f \times \mathrm{VWC}$. We estimated vegetation water content following the method used in the SMAP SM retrieval algorithm (Chan et al., 2013):

$$\mathrm{VWC} = 1.9134 \times \mathrm{NDVI}^2 - 0.3215 \times \mathrm{NDVI} + stem_{factor} \times \frac{\mathrm{NDVI}_{max} - \mathrm{NDVI}_{min}}{1 - \mathrm{NDVI}_{min}} \tag{10}$$

The maximum (NDVI_{max}) and minimum (NDVI_{min}) NDVI values were extracted from the MODIS 16-day NDVI record (MOD13A2). The $stem_{factor}$ was used to estimate the stem water content, which varies from 1.5 to 3.0 for grasslands to open shrublands. Soil emissivity (e_p) was related to soil reflectivity (r_p) by $e_p = 1 - r_p$, and the roughness parameter was used to correct the smooth surface reflectivity r_{s_p} for rough surfaces as in $r_p = r_{s_p} e^{-h}$. The r_{s_p} values were calculated based on the surface soil dielectric constant using the dielectric model developed in Park et al. (2017, 2019), with surface (~3 cm) SM and temperature inputs simulated by the PWBM model. A brief description of the Park's model is given in Appendix A. The Park's model generally captures the difference between organic and mineral soils as other models (Figure S3 in Supporting Information S1), but allowing for a fully coupling with hydrologic models such as PWBM. We optimized the roughness parameter, VOD, and the two vegetation parameters (b_f and $stem_{factor}$) as described in Section 3.3. Finally, the effective soil temperature (T_{eff}) required in the tau-omega model was calculated as the weighted average of the PWBM model simulated surface (~3 cm, center depth of layer 2) temperature (T_{surf}) and deep (55 cm, center depth of layer 8) soil temperature (T_{deep}) as in Wigneron et al. (2008) and Gao et al. (2018):

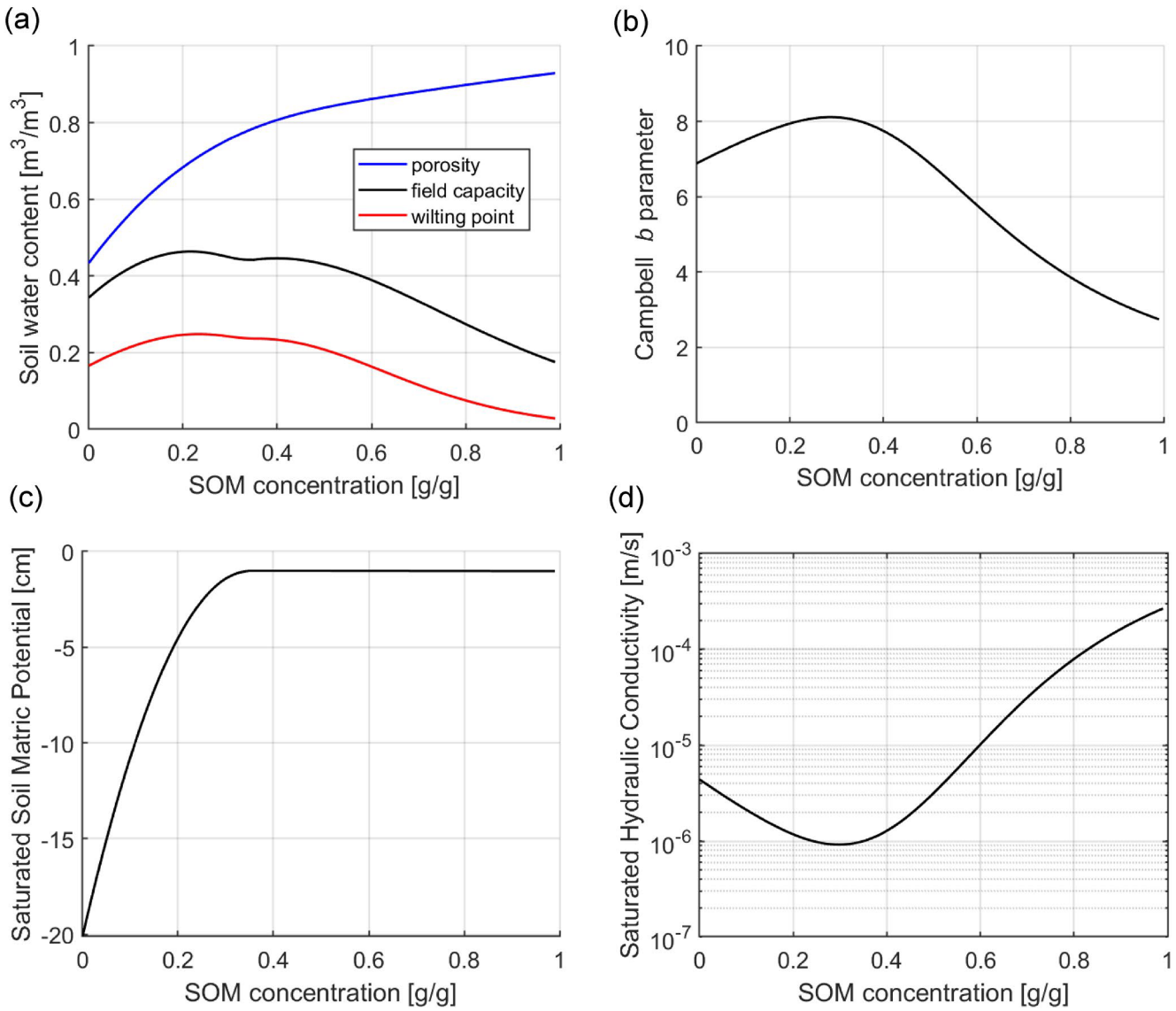

Figure 3. Selected key model hydraulic parameters in relation to SOM variations. The hydraulic parameters for the fibric peat (SOM = 1) and sapric peat (SOM_1 = 35%) defined as in Table S1 in Supporting Information S1 were used to solve the hydraulic parameters for soils with varying SOM conditions. The mineral soil texture has 44% sand fraction and 25% clay fraction. The field capacity was calculated with matric potential of 100 pa.

$$T_{eff} = T_{deep} + (T_{surf} - T_{deep}) \times \left(\frac{\theta}{0.398}\right)^{0.181} \tag{11}$$

where θ is the surface (~3 cm) SM (cm^3/cm^3).

3.3. Model Calibration and Validation

We used a two-step calibration approach in this study. Since soil hydraulic parameters are closely related to the SOM concentration (Figure 3), we first calibrated the SOM profile used in the hydrology model, and then calibrated the tau-omega parameters using the SMAP Tb data. The tau-omega model was only run for the thaw season due to a lack of understanding of the scattering process in frozen soils (Roy et al., 2017). For all optimization runs, the cost function was defined as the Root Mean Square Errors (RMSE) between model simulated and observed values.

The PWBM hydrology model was calibrated and validated using in situ soil temperature and moisture, and evapotranspiration data from the three Imnavait Creek tower and neighboring sites. The surface meteorology inputs for the PWBM model include daily mean and minimum air temperature, downward solar radiation, and vapor pressure deficit, which were mainly extracted from the Daymet record (Thornton et al., 2020), except that windspeed data were extracted from MERRA2 reanalysis data. Precipitation in the regional data sets generally has large uncertainty in the Arctic region. Therefore, we used precipitation measurements from the Imnavait Creek SNOTEL site, with gaps in the daily measurement record filled from the corresponding daily Daymet record.

For the hydrology model calibration, we used the following exponential decay function, similar to Chen et al. (2020), to characterize the SOM distribution along the soil vertical profile:

$$\mathrm{SOM}(z) = \mathrm{SOM}_0 + \frac{K_0 - \mathrm{SOM}_0}{\sqrt{1 + e^{-B(z - z_{org})}}} \tag{12}$$

where SOM_0, and K_0 are the SOM values (g/g) when z approaches the values of $-\infty$ and $+\infty$, respectively. B is the decay rate (m^{-1}), which is generally close to 50 m^{-1} based on in situ data (Chen et al., 2020). Z_{org} is the depth at which the maximum decay rate (or organic-to-mineral transition) occurs. We used the simulated annealing (SA) method (Goffe et al., 1994) to optimize the unknown parameters, including SOM_0, K_0 and Z_{org}. Generally, the SOM value at the soil bottom is very low. Test optimization runs using three parameters also showed the optimized K_0 value at the study site to be a very small value. To minimize the amount of time for the SA optimization, we set K_0 to a constant value (0.05 g/g), which was also used in Chen et al. (2020). We then performed four calibration experiments for the parameter optimization. The first two experiments used surface soil temperature (T_{soil}) or SM data only to optimize the two remaining SOM parameters. We then optimized the parameters using T_{soil} at multiple soil depths, and finally optimized the parameters using both surface T_{soil} and SM data. We did not optimize the parameters using SM at multiple depths because the SM measurements are generally associated with large uncertainties in the Arctic and deep SM data are particularly scarce. We used equal weighting for the cost function when using soil temperature or moisture only. When using T_{soil} and SM data together, to determine the weight for different cost functions, we first calculated the RMSE values of model simulated and observed T_{soil} and SM separately, and then adjusted the weighting to make the RMSE values for both variables approximately equal, in order to give similar weight to the T_{soil} and SM observations.

With the SOM parameters calibrated, the PWBM model simulated soil moisture and temperature were then converted to soil dielectric constant and used as inputs to the tau-omega model. For the tau-omega model calibration, we also used a two-step approach. First, we ran the model using a constant VOD value throughout the thaw season and optimized the VOD and soil roughness parameters. Assuming the resulting VOD value was close to the mean value for the thaw season, we then selected the b_f and $stem_{factor}$ parameters (Equation 10) that gave the best solutions for model simulated Tb. Previous studies have shown different values for both VOD (or b_f values) and roughness parameters at H and V pol (DeLennoy et al., 2013; Kerr et al., 2012). However, we found that accounting for these differences did not significantly improve the optimization results; therefore, we used the same VOD and roughness parameters for both H and V pol.

4. Results

4.1. Soil Moisture Drydown Analysis

The drydown timescale (τ_0) derived from in situ SM data is generally consistent with the value extracted from the SMAP PR data during the early thaw period (Figure 4), except for the Kelly Station (KLS) SNOTEL site (Figure S4 in Supporting Information S1). The KLS site has more precipitation than all other sites, with mean annual precipitation of 419 mm from 2013 to 2019, which makes it relatively difficult to find representative drydown periods during the short thaw season. The data at this site also show a poor fitting for the SM drydown curve ($R = 0.56$). The 36-km EASE2 grid encompassing the Prudhoe Meadow (PM) site has a much smaller surface open water fraction (~3%), compared with the 9-km EASE2 grid encompassing this site. Therefore, Tb data extracted from the SMAP 36-km EASE2 grid product was used here. The derived drydown timescale was shortest at the Happy Valley (HV) site, and longest at the PM site, while our field surveys indicate higher surface SOC content at the HV and IMN sites, and lower SOC content at the PM site.

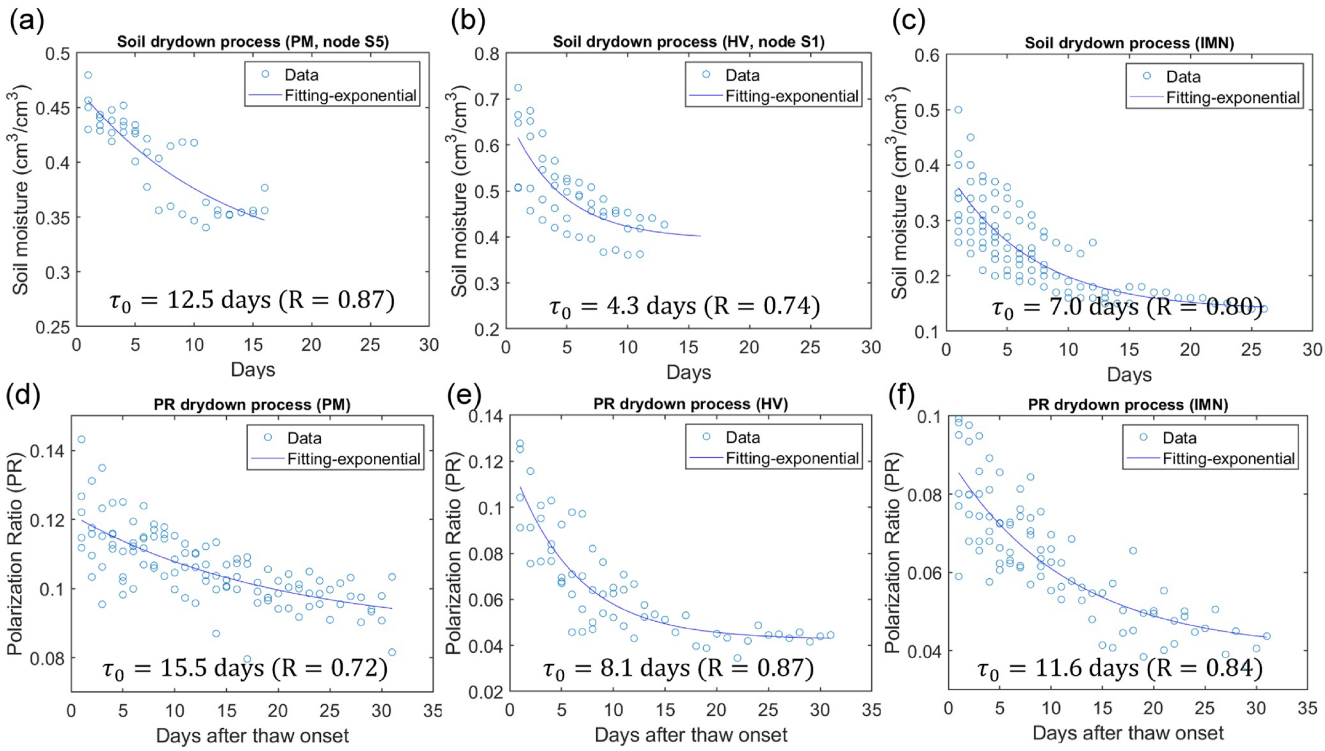

Figure 4. SM drydown trends (a–c) extracted from in situ data, and (d–f) indicated by the SMAP PR data after spring thaw onset, at the SoilSCAPE (PM, HV) and SNOTEL sites (IMN).

At the regional scale, the soil drydown timescale derived from the SMAP PR data were significantly ($p < 0.01$) correlated with the SoilGrids surface (0–5 cm) SOC concentration (SOCC) and soil bulk density data (Figure 5). Higher SOCC or lower soil bulk density was associated with a shorter drydown timescale. Overall lower correlation was found between the drydown timescale and soil bulk density compared with the SOCC data. Comparisons of the Alaska-wide in situ soil carbon data with the SoilGrids data indicates an overall better accuracy of the SOCC data ($R = 0.84$) than the soil bulk density data ($R = 0.58$) for both versions of SoilGrids products.

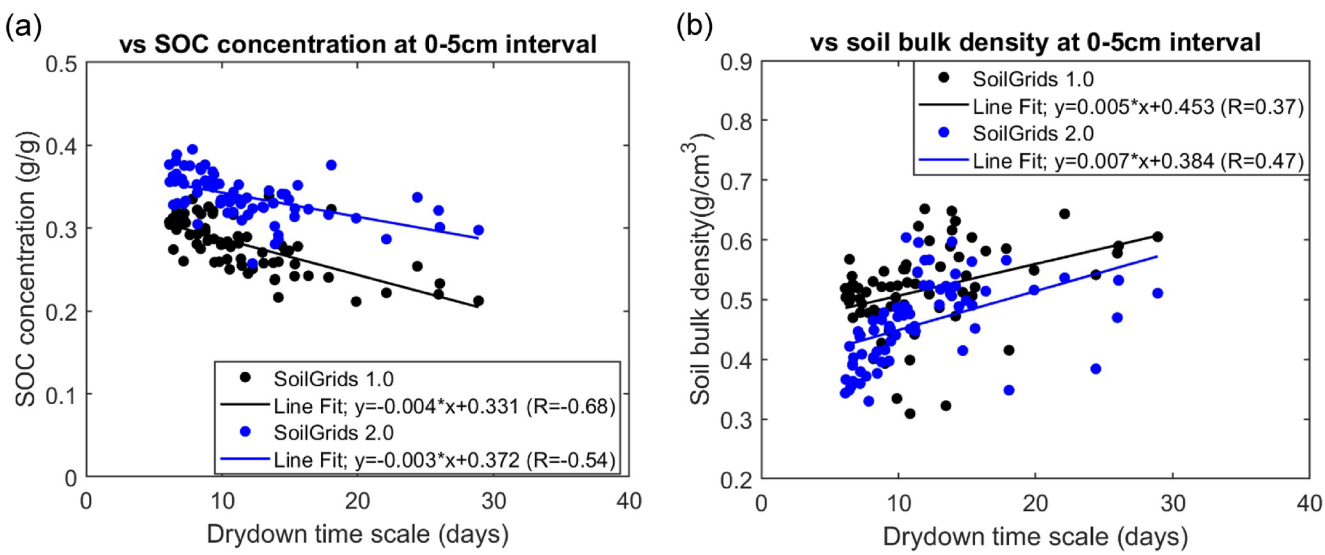

Figure 5. Correlation between the drydown timescale derived from SMAP PR data during the early thaw period and SoilGrids surface SOC concentration and soil bulk density in the DHN subregion (Figure 1b).

Table 2
Statistics of Estimated Drydown Timescale Derived From SMAP PR Observations and SoilGrids Soil Carbon Data for the Two Dominant Tundra Types in the DHN Region

		Soil bulk density (0–5 cm, g/cm^3)		SOCC (0–5 cm, g/g)	
	Drydown time scale (days)	version 1	version 2	version 1	version 2
lc = 51 (num* = 49)	10.10 ± 3.77	0.49 ± 0.07	0.44 ± 0.06	0.29 ± 0.03	0.34 ± 0.03
lc = 72 (num* = 22)	15.10 ± 5.85	0.57 ± 0.04	0.51 ± 0.06	0.25 ± 0.02	0.32 ± 0.02

Note. *indicates the number of 9-km EASE2 grid cells representing each NLCD land cover type, with lc = 51 representing scrub/shrub tundra and lc = 72 representing herbaceous/sedge tundra. Grid cells with poor data fitting ($R < 0.75$) were excluded, accounting for 22% of the area. For all grid cells included, the open water fraction is below 0.4% (mean = 0.1%), and the mean slope is 1.5%.

Previous studies also pointed out larger uncertainties in the soil bulk density from regional and global data sets (Tifafi et al., 2018). For the soil drydown analysis, we excluded the 9-km EASE2 grids with more than 1% of surface open water, and also grid cells with dominant land cover types other than tundra. In addition, we excluded grid cells with a poorly fit SM drydown curve ($R < 0.75$), indicating unreliable estimates of drydown parameters. When using a higher threshold for the data fitting correlation (e.g., 0.80), the correlation between the drydown timescale and soil carbon data was improved for both SOCC and soil bulk density. Significant ($p < 0.1$) differences in the drydown timescale and soil carbon properties were found between the two dominant tundra types in this region, with shorter drydown time and higher SOCC in shrub (versus sedge) tundra (Table 2). Much lower correlation was found between the estimated drydown timescale and other variables including elevation, slope, and soil sand and clay content.

4.2. Modeling Calibration and Validation

4.2.1. Hydrologic Modeling

The hydrology model was calibrated using in situ T_{soil} and SM data from 2012 to 2014, and was then validated using data obtained during other time periods. The SOM profile calibrated using different combinations of in situ T_{soil} and SM data sets is generally similar, with the mean surface (0–5 cm) SOM ranging from 0.66 to 0.82 (Table 3), which corresponds to SOCC ranging from 0.38 to 0.48 assuming 58% carbon content for soil organic matter (Pribyl, 2010). Model calibration derived using the soil temperature data (Run1 and Run2) produced the largest reduction in RMSE values in the model simulations, while the model calibration conducted using surface SM data alone (Run3) shows the least RMSE reduction. These results can be attributed to large variability in the SM data and larger uncertainties in both SM observations and model simulations over Arctic tundra. Even though the model calibration derived using T_{soil} at multiple layers (Run2) provides slightly better T_{soil} simulations, the model simulated SM values using the calibrated SOM values show a large positive bias. Therefore, we chose the calibrated SOM values in Run1 as the optimal parameters. If we assume soils with SOM > 80% (corresponding to FC > 57% and SOCC > 46%) as the pure organic layer, the depth of the surface organic layer is ~3.5 cm using the above calibrated SOM profile, which is close to the soil characterization at the dry heath tundra tower site and the IMN SNOTEL site.

Table 3
Calibration Experiments for the PWBM Model and the Reduction in Model Errors Compared With Initial Model Runs

	Target variables	SOM_0 (g/g)	Z_{org} (m)	SOM (0–5 cm, g/g)	RMSE reduction
Run1	Surface T_{soil}	0.95	0.11	0.82	63%
Run2	T_{soil} at 5, 34, and 50 cm	0.95	0.07	0.66	71%
Run3	Surface SM	0.89	0.10	0.75	20%
Run4	Surface T_{soil} and SM (weight: [0.1 1])	0.91	0.11	0.80	40%

Note. The model calibration period is from 2012 to 2014. For the parameter optimization, SOM_0 ranges from 0 to 1.0, and Z_{org} ranges from 0 to 0.5, with additional constraint of $SOM_0 + Z_{org} < 1.2$ to avoid a very thicker organic layer with high SOM concentration, which can result in unstable hydrologic model solution.

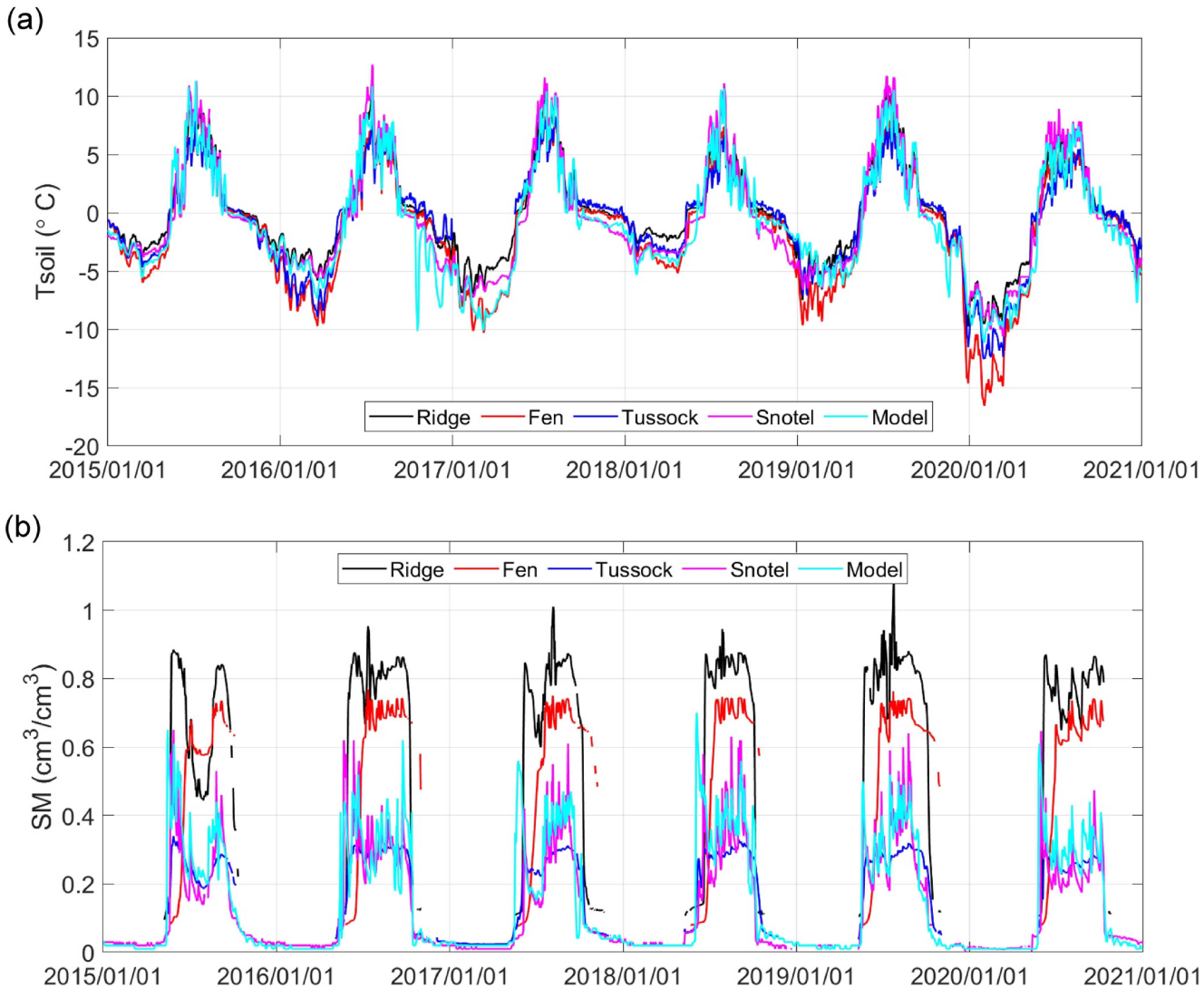

Figure 6. Daily time series of model simulated surface T_{soil} and SM during the validation period (2015–2020), compared with in situ observations at the three EC tower sites and IMN SNOTEL site. Large drops in the model simulated T_{soil} in early winter of 2016 is likely due to a dry bias in the Daymet precipitation used during this period.

Model simulated surface T_{soil} and SM are generally consistent with observations at the Imnavait Creek site (Figure 6). Model simulated T_{soil} has a mean bias of ~−0.5°C and RMSE lower than 1.5°C during the calibration period (Table 4). There is a slight increase in the RMSE values for T_{soil} during the validation period. The model

Table 4
Statistics of Model Simulated T_{soil} at the Imnavait Creek Site During the Calibration (2012–2014) and Validation Periods

	T_{soil} (5 cm, °C)			T_{soil} (34 cm, °C)			T_{soil} (50 cm, °C)		
	R	Bias	RMSE	*R*	Bias	RMSE	*R*	Bias	RMSE
Cal period	0.98 ± 0.00	–0.57 ± 0.33	1.35 ± 0.27	0.97 ± 0.01	–0.41 ± 0.57	1.16 ± 0.15	0.97 ± 0.01	–0.52 ± 0.55	1.21 ± 0.15
Val period	0.96 ± 0.02	–1.00 ± 0.31	1.66 ± 0.28	0.96 ± 0.01	–0.33 ± 0.50	1.40 ± 0.52	0.95 ± 0.01	–0.43 ± 0.48	1.42 ± 0.45

Note. For surface T_{soil}, the data at the heath tundra tower site was used, and the validation period is from 2008 to 2011, and from 2015 to 2020. The other sites including the IMN SNOTEL site, except for the wet sedge tundra (with a positive bias in the model T_{soil}), show similar performance. For T_{soil} at depth, the validation period is from 2008 to 2011, and 2015.

Table 5
Statistics of Model Simulated SM at the Imnavait Creek Site During the Calibration (2012–2014) and Validation Period

	SM (5 cm, cm^3/cm^3)			SM (14 cm, cm^3/cm^3)			SM (39 cm, cm^3/cm^3)		
	R	Bias	RMSE	*R*	Bias	RMSE	*R*	Bias	RMSE
Cal period	0.81 ± 0.11	–0.02 ± 0.03	0.09 ± 0.02	0.95 ± 0.02	–0.02 ± 0.01	0.08 ± 0.01	0.95 ± 0.03	–0.03 ± 0.01	0.07 ± 0.01
Val period	0.87 ± 0.06	0.01 ± 0.03	0.08 ± 0.02	0.94 ± 0.01	–0.01 ± 0.02	0.09 ± 0.01	0.93 ± 0.02	–0.03 ± 0.02	0.07 ± 0.01

Note. For surface SM, the SNOTEL site data was used for model validation due to larger soil measurement uncertainty at the tower sites, and the validation period is from 2015 to 2020. For SM at depth, the validation period is from 2008 to 2011, and 2015.

simulated deep T_{soil} shows similar accuracy compared with surface T_{soil}. The model simulated T_{soil} generally shows larger errors during the winter period than the thaw season (Figure 6a), which is mainly due to uncertainties in the model simulated snowpack and associated snow insulation effects, with additional uncertainties contributed from the input precipitation data. For example, Daymet precipitation was used in most of year 2016, due to extended gaps in the SNOTEL precipitation data. Daymet precipitation is much lower than SNOTEL during the winter period, which results in large drops in the T_{soil} simulations in the early winter of 2016. Model simulated SM shows comparable accuracy during both calibration and validation periods (Figure 6b and Table 5). There are larger uncertainties in surface SM data at the three EC tower sites, including SM occasionally greater than 100%, and unrealistic surface soil saturation values during the thaw season at the relatively dry heath tundra sites (Figure 6b). Therefore, we used the surface SM at the SNOTEL site for comparison. Model simulated surface SM shows good correspondence with the in situ data ($R \geq 0.91$, RMSE ≤ 0.09 cm^3/cm^3). The deep SM data show much less variability and stay saturated for most of the thaw season; while the associated accuracy is mostly due to changes in the SOM concentration (affecting the soil porosity) and model simulated freeze/thaw transition timing.

Model simulated ET was closely related to model simulated SM time series or vice versa. The model simulated ET show overall good consistency with the tower-based observations, although large scattering was observed during both the thaw and frozen seasons (Figure S5 in Supporting Information S1). The missing data period in the latent heat flux measurements can account for more than 45% of the observational period; therefore, the accuracy of the gap-filling method can have a large impact on the ET measurements. After gap-filling, the tower ET records showed a large decreasing trend (~9.25 mm/yr, $p < 0.01$) throughout the observation period (2008–2020), and we cannot exclude this trend from the uncertainty in the data gap-filling methods. The annual ET during the early period (2008–2012) ranged from 178 to 194 mm/yr at the three tower sites and seems more consistent with observations in other Arctic regions (Euskirchen, Edgar, et al., 2017), compared with a much lower value during the later period (126–140 mm/yr). Therefore, we mainly chose the 2008–2012 period for model validation. For the 2008 to 2012 period, the respective *R*, bias and RMSE values for the model simulations are 0.85 ± 0.05, −0.15 ± 0.16 mm/day, and 0.42 ± 0.06 mm/day at the heath tundra tower based on the nongap-filled tower observations, with similar accuracy at the wet sedge tundra tower site. Model accuracy at the tussock tundra site is lower, with respective *R*, bias, and RMSE values of 0.75 ± 0.09, −0.50 ± 0.41 mm/day, and 0.42 ± 0.06 mm/day. The resulting ET RMSE values are within the uncertainty range of the three tower data sets. During the later period, the model simulated ET still shows a high correlation with the tower-based measurements ($R \geq 0.82$), but with a larger positive bias (~0.18–0.21 mm/day). Additional investigation is ongoing to understand the negative trend in the ET data. Finally, a more sophisticated snow sublimation scheme is needed, as the model does not adequately capture the observed large ET variations attributed to snow sublimation and does not represent snow deposition. However, these additional factors are beyond the scope of this study.

4.2.2. Tb Modeling

Vegetation optical depth (VOD, τ_p) and roughness (h) can have compensating effects on the model simulated Tb; that is, a large VOD or roughness value can both result in high emissivity and thus higher Tb values. Without additional constraint on the tau-omega model parameters, we obtained a rather high VOD (≥0.5) and low roughness (~0.06), which is unrealistic at this tundra site. Therefore, we limited the maximum VOD to 0.4, resulting in model optimized VOD of 0.396 and roughness of 0.192. We also obtained two additional sets of

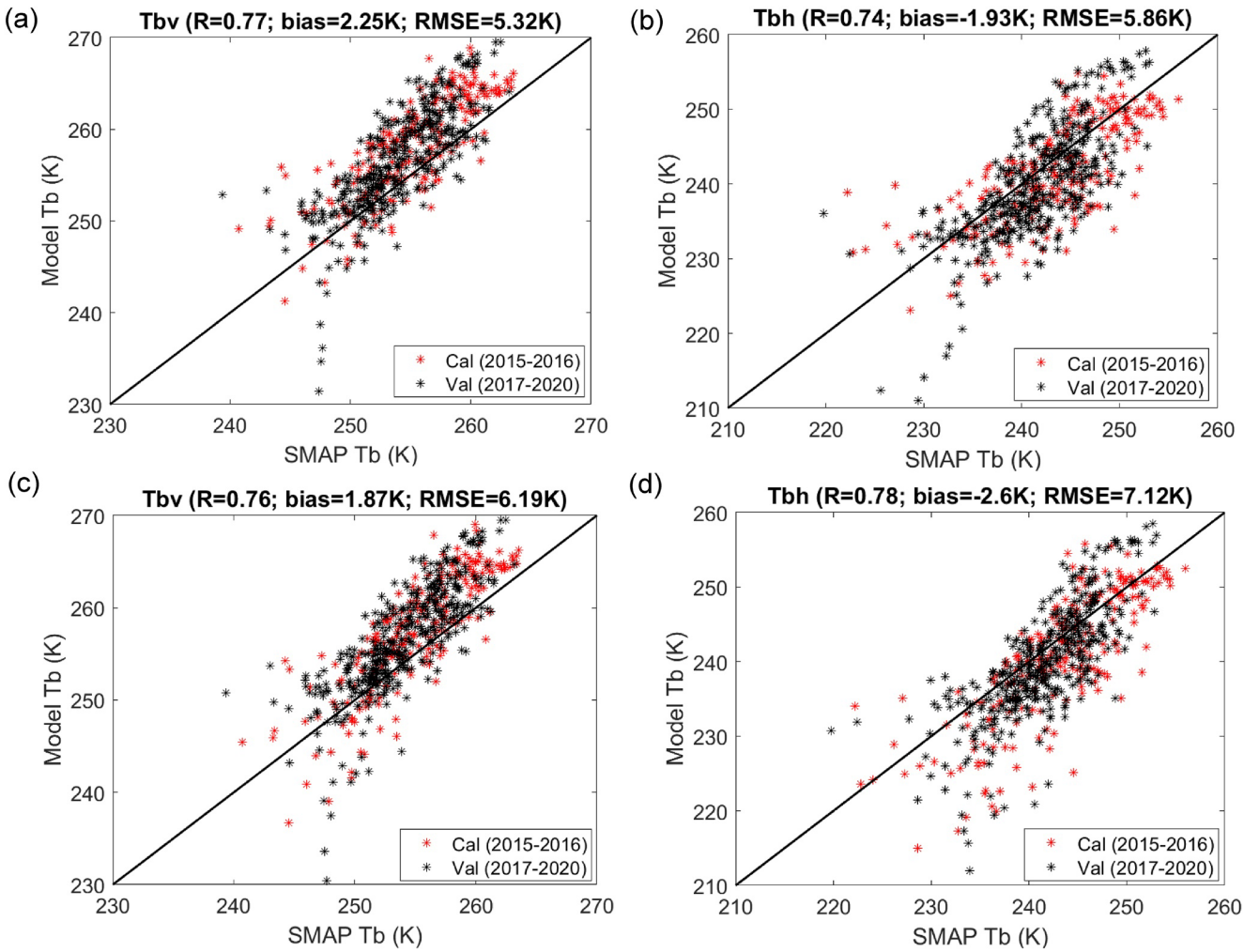

Figure 7. Scatter plots of model simulated daily T_{bv} (a, c) and T_{bh} (b, d) for the calibration (Cal, 2015–2016) and validation (Val, 2017–2020) periods, using mean VOD of 0.35 (a)–(b), and accounting for temporal changes in the vegetation water content and VOD values during the thaw season (c, d).

optimal parameters by limiting the VOD value to different ranges (Table 6), which gave slightly larger RMSE values for the Tb estimates. VOD lower than 0.3 gives substantially large RMSE values; therefore, we did not conduct optimization with VOD < 0.3. The model simulations showed slightly larger errors when accounting for vegetation water content changes using Equation 10, compared with model simulations derived using a constant VOD value throughout the thaw season. For this calibration, we limited the $stem_{factor}$ to the [1.5 2.0] range based on the SMAP ancillary data report (Chan et al., 2013). For a mean VOD value of 0.35, the calibrated values for $stem_{factor}$ and b_f are 1.80 and 0.21, which gives a mean estimate of 1.61 kg/m^2 for vegetation water content from June to August. The shrub tundra in our study area has a mean aboveground biomass of ~0.97 kg/m^2 (Berner et al., 2018), indicating that the above value is a reasonable estimate. A higher VOD value such as 0.4, allows for higher vegetation water content estimates, which, may be too high in this region. Model simulations using a lower VOD value such as 0.3, have RMSE values increasing faster when accounting for temporal changes in vegetation water content and VOD, which also shows a large positive bias in the T_{bv} simulations. Therefore, for the sensitivity analysis discussed below, we used the model simulations derived using a mean VOD value of 0.35.

Figure 7 shows the scatter plots of model simulated brightness temperature with SMAP data throughout the entire SMAP observational period (2015–2020) using the mean VOD value of 0.35. Model simulated T_{bh} has slightly higher RMSE values (6–7 K) than the T_{bv} (5–6 K) simulations. Model simulated T_{bv} generally shows a positive bias relative to the SMAP data, while T_{bh} generally shows a negative bias especially for lower Tb values. The biases may be reduced through using different values of VOD or roughness for the H and V pol. The model

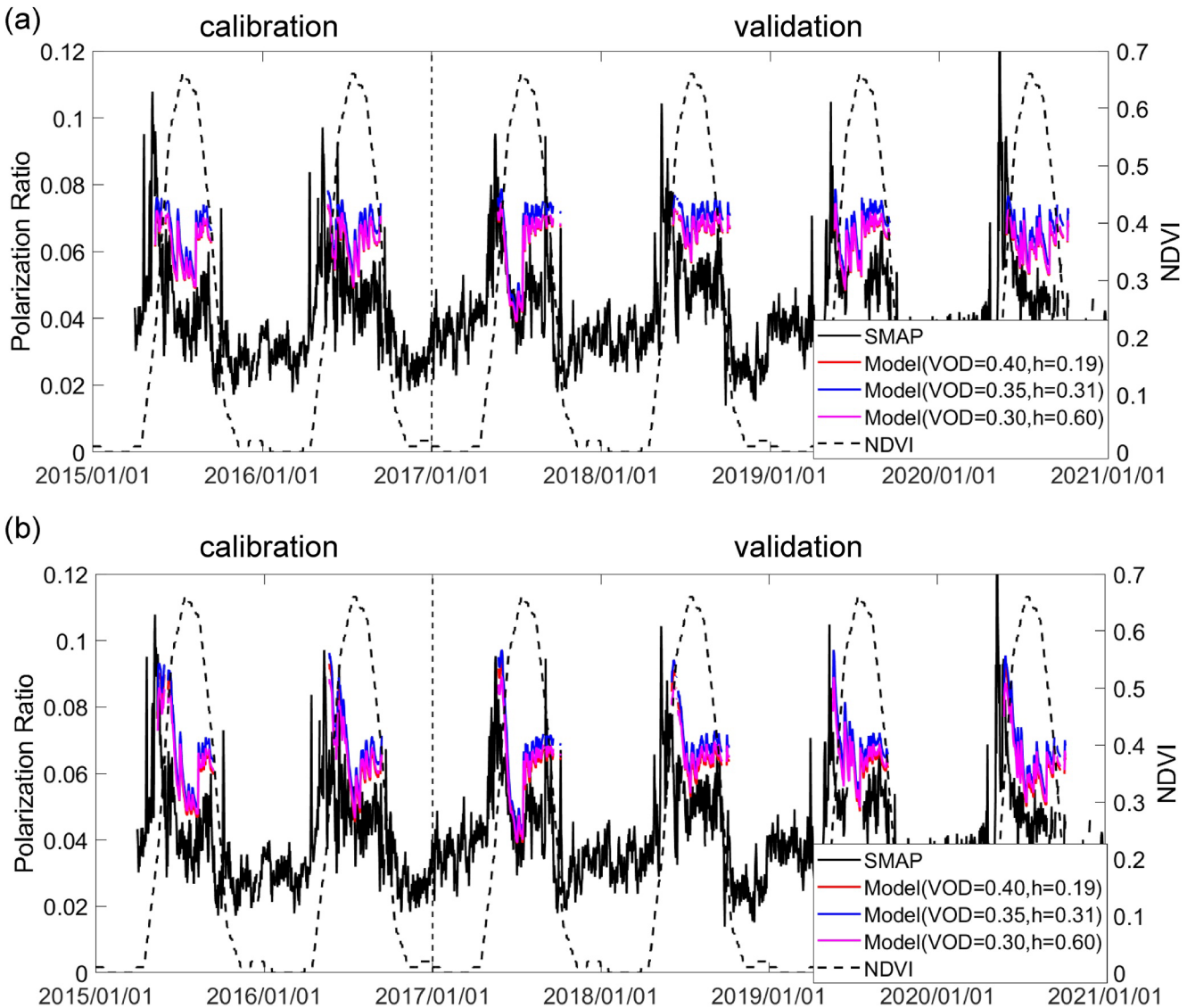

Figure 8. Daily time series of MODIS NDVI and SMAP polarization ratio (PR) measurements compared with model PR simulations derived using different mean VOD and roughness parameters (a), and accounting for temporal changes in vegetation water content and VOD during the thaw season (b) over the Imnavait Creek tower site. The calibration period is from 2015 to 2016, and the validation period is from 2017 to 2020.

simulated PR shows a better correlation and temporal consistency with the SMAP data (Figure 8) when using temporally varying VOD values accounting for vegetation water content changes throughout the thaw season (Equation 10). The correlation between model simulated and SMAP PR data is 0.64 with time-varying VOD values and 0.42 using a mean VOD value, with both correlations significant at p level of 0.01. There were no significant differences among the model simulated PR time series using different combinations of VOD and roughness parameters due to compensating effects of VOD and roughness on brightness temperature and PR. The model generally overestimated the SMAP PR value during the later thaw season (starting around DOY 220). During this period, surface soil is generally wetter than the previous peak season dry period (Figure 6b) due to greater precipitation and reduced evaporation (Figure S5 in Supporting Information S1). In addition, vegetation senescence also starts around mid-August; therefore, we would expect vegetation water content to decrease accordingly. Thus, the model generally simulated a higher PR value during that period. However, increasing surface litter during the senescence period with wetter surface conditions may increase the microwave attenuation (i.e., increasing VOD values) and thus decrease the PR sensitivity to surface SM conditions (Kerr et al., 2012), which was not accounted for by the model.

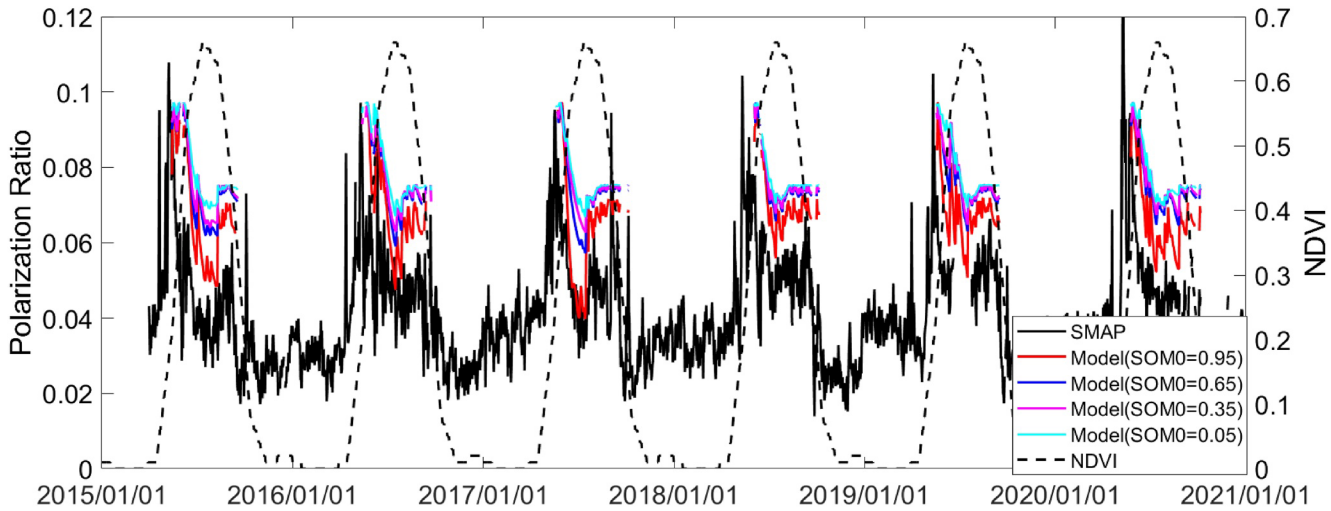

Figure 9. Model simulated sensitivity of L-band polarization ratio (PR) daily time series to different surface SOM conditions through varying SOM_0 values in Equation 12. The SOM concentration in the top 5 cm layer is 0.84, 0.57, 0.31, and 0.05 corresponding with SOM_0 values of 0.95, 0.65, 0.35, and 0.05, respectively. The simulations were conducted accounting for temporal changes in vegetation water content and VOD values during the thaw season, with a mean VOD value of 0.35 (roughness = 0.31). Model results are plotted with SMAP PR and MODIS NDVI records for the Imnavait Creek tower site.

4.3. Sensitivity of L-Band Polarization Ratio to Surface Organic Soil Concentration

We investigated the sensitivity of model simulated L-band PR to surface SOM conditions by comparing the model simulated PR time series using different SOM_0 values in the SOM profile (Equation 12). For consistent comparison, we kept Z_{org} and K_0 values the same as the above simulation, while changes in SOM_0 result in associated changes in the surface SOM concentration (or SOCC). Figure 9 compares the model simulated L-band PR time series for surface organic soils with high, medium, and low SOM concentrations, in addition to the mineral soils. For the mineral soil conditions, we assumed that surface SOM_0 is equal to SOM at depth, when the SOCC is ~2.9% with $K_0 = 5\%$. The resulting model simulated PR is most sensitive to surface SOM changes when surface SOM_0 value is high. The PR changes during the early thaw period are reduced when surface SOM is lower. The differences in the model simulated PR are larger when there was a significant drying period such as in year 2015 and 2017, indicated by the surface SM conditions (Figure 6b).

To further understand the sensitivity of the L-band PR during the spring thaw period, we simulated the PR response to SM variations in different SOM conditions. We first calculated the brightness temperature and PR values at two extreme SM conditions, when soil is saturated (at porosity) and at wilting point, respectively, using the tau-omega model and the new soil parameterization described in Section 3.1.1, with different SOM input values. We then calculated the PR changes between these two conditions. This is used to simulate the surface soil wetness conditions during the early thaw period when surface soil progresses from near-saturation to dry conditions with increases in soil drainage and evapotranspiration. The estimated PR response to different SOM, VOD, and roughness conditions are shown in Figure 10. For comparison, we also included results derived using different dielectric models. Large changes in the PR were observed for soils with higher SOM concentration. However, the results did not show significant changes in the PR values until SOM reaches about 30–40% (~17.4–23.2% for SOCC), which was consistent with the above coupled model sensitivity analysis. Higher VOD or roughness values reduced the sensitivity of Tb and PR to surface SM changes. Similar behavior in the model simulated L-band PR was observed if the surface SM changes from field capacity to wilting point, albeit with smaller magnitude in the PR changes (Figure S6 in Supporting Information S1). Soil texture also affects the PR sensitivity to SM variability under different SOM concentrations (Figure S7 in Supporting Information S1), mainly due to its influences on the Campbell *b* shape parameter (Figure 3). In coarser soils, PR changes can be similar between sandy mineral soils and soils with a lower amount of SOM. However, regardless of soil texture, the PR is most sensitive to SM at high SOM concentration (SOM > 60%, or SOCC > ~34.8%).

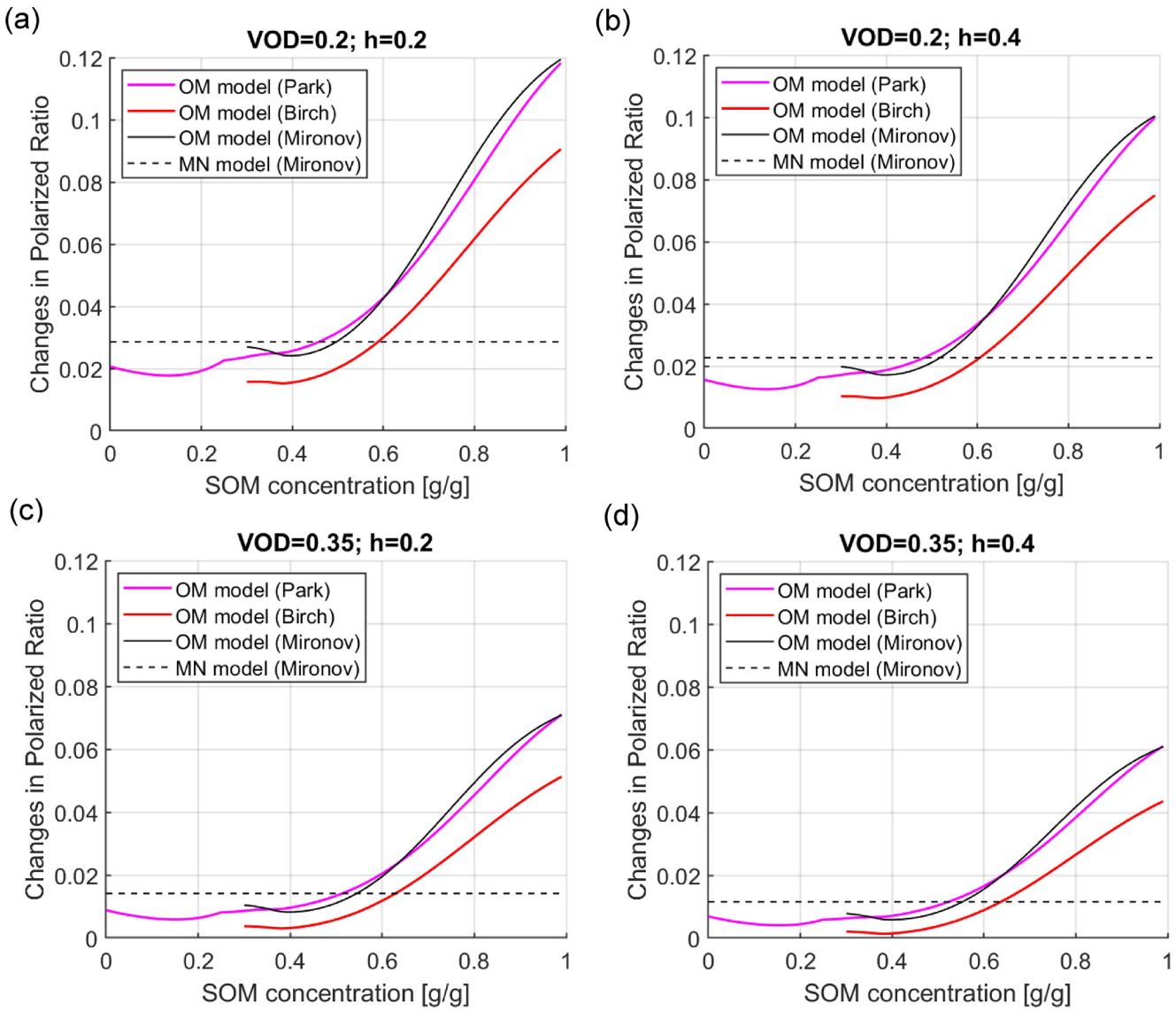

Figure 10. Changes in the L-band polarized ratio in response to SM variability between saturation and the wilting point for different SOM concentrations, simulated using the tau-omega model with different VOD and roughness values. This simulation uses soil texture similar to the Imavait Creek tundra study site (sand = 44%, clay = 25%). The roughness (h) at H and V pol are assumed equal. Different dielectric models accounting for organic matter (OM), and for mineral soil only (MN, Mironov et al., 2009) were used to simulate the dielectric constant response to SM changes. The two OM models (Bircher et al., 2016b; Mironov et al., 2015) do not apply to soils with low SOM concentration; therefore, the simulations with SOM < 35% were not included.

5. Discussion

5.1. Soil Moisture Drydown Characterization in the Arctic Region

Using the polarization ratio as a proxy for surface SM, the soil drydown timescale derived from SMAP polarization ratio data during the early thaw period shows strong correlation with both surface SOC concentration and soil bulk density obtained from SoilGrids for a relatively flat Arctic tundra area. Previous studies have related SM drying rates to soil texture, soil sensing depth, and surface evapotranspiration in other regions (Kurc & Small, 2004; McColl et al., 2017; Rondinelli et al., 2015; Shellito et al., 2016). These studies also pointed out that different factors may play dominant roles in different climate regions, and can vary during different stages of the soil drydown period (McColl et al., 2019). The soil drydown rate near soil saturation is mainly controlled by the soil drainage rate, while the subsequent soil drying process is mostly controlled by soil evaporation. Depending on the SM, soil evaporation rate can change and thus affect the soil drydown rate.

Table 6
Statistics of the Tau-omega Model Simulated Brightness Temperatures Derived using Different Sets of VOD (τ_p) and Roughness Parameters During the Calibration period (2015–2016)

	Mean $\tau_p = 0.40$, $h = 0.19$			Mean $\tau_p = 0.35$, $h = 0.31$			Mean $\tau_p = 0.30$, $h = 0.60$		
	R (K)	Bias (K)	RMSE	R (K)	Bias (K)	RMSE	R (K)	Bias (K)	RMSE
T_{bh} Constant τ_p	0.75	–0.62	4.97	0.75	–1.72	5.36	0.75	–0.22	4.97
T_{bh} Varying τ_p	0.82	–1.62	5.78	0.81	–2.63	6.24	0.81	–0.50	5.26
T_{bv} Constant τ_p	0.81	2.99	4.66	0.81	2.77	4.67	0.81	4.00	5.38
T_{bv} Varying τ_p	0.83	2.44	4.94	0.83	2.27	4.99	0.83	3.60	5.45

Note. For the "constant τ_p" scenario, a mean τ_p value was used throughout the thaw season, while for the "varying τ_p" scenario, temporal changes in the vegetation water content and τ_p values were represented, with the same mean τ_p value during the thaw season.

Similar processes may also control soil drying rates in Arctic tundra. Both the drainage rate and soil evaporation capacity are closely related to soil hydraulic properties, which are mainly affected by the soil organic carbon content and decomposition state (Bechtold et al., 2019; Letts et al., 2000; Verry et al., 2011). Soil carbon content and decomposition state can show large variations along depth in Arctic soils, leading to large variability in the soil hydraulic properties, which, together with a shallow thaw depth, can exert strong control on the soil water transfer (Quinton et al., 2000) and affect the L-band penetration capability. Our modeling experiment indicates that organic soils with higher fiber content (SOM > 60% or FC > 33%) generally have a higher saturated hydraulic conductivity, and lower water-retention capacity (Figure 3), which can lead to rapid loss of water. A larger amount of water is also available for discharge or evaporation due to a larger difference between the soil porosity and wilting point. Field experiments also generally show rapidly drying and wetting features in less decomposed organic soils with more fibrous SOM (Zwieback & Berg, 2019).

However, other factors may also play important roles in controlling SM drydown rates in the Arctic. Local topography controls the soil drainage rate, and can have significant impact on the soil drydown process. Although our study area is generally flat, with mean slope of ~1.5%, additional investigation is needed to separate the effects of soil properties from other confounding factors influencing SM dynamics in regions with more complex topography. Another important factor affecting surface soil drydown in permafrost areas is the thawing process, with increasing soil thaw depth promoting soil water drainage to deep soils (Vonk et al., 2019). However, during the early thaw period, a shallow thaw depth or water table restricts vertical water movement; lateral preferential flow can form in the porous organic layer and is an important mechanism of water transmission during this period (Quinton et al., 2000; Woo & Marsh, 2005). Microtopography and spatial heterogeneity in the organic soil properties also affect water storage, flow paths and heat transfer, and thus affect soil thaw and drainage rates (Kurylyk et al., 2016; Quinton & Marsh, 1998; Shi et al., 2015). How to quantify the effects of the above processes on surface SM drying during the early thaw season needs further investigation.

Uncertainties may be also associated with our analysis of soil drydown timescale at the regional scale. We used the L-band PR as a SM proxy during the early thaw season in the regional analysis. Although we focus on the early thaw period when vegetation water content is relatively low compared with the peak thaw season, the changes in vegetation water content and VOD during the growing season can affect the sensitivity of L-band PR to surface SM conditions. Using direct SM retrievals rather than the PR values will help to better understand the underlying processes. However, reliable SM estimates from spaceborne sensors are currently lacking in the northern permafrost region (Wrona et al., 2017; Zwieback & Berg, 2019). A major reason for this uncertainty is due to challenges in characterizing the organic soil hydraulic and dielectric properties, which affect soil moisture retrieval accuracy as discussed below. Seasonal transient waterbodies in the northern permafrost region are common, and can have significant impact on surface emissivity, imparting a wet bias into surface SM retrievals without correcting for this effect. In addition, instead of using the tau-omega model, using a more detailed forward emission model such as the two-stream emission model (Schwank et al., 2018) accounting for multiple or volume scattering processes between the vegetation/litter layer and surface soil, will likely allow for better VOD and SM estimates in the Arctic.

Table 7
Same as Table 6, but the Statistics was Calculated for the Validation Period (2017–2020)

	Mean $\tau_p = 0.40$, $h = 0.19$			Mean $\tau_p = 0.35$, $h = 0.31$			Mean $\tau_p = 0.30$, $h = 0.60$		
	R (K)	Bias (K)	RMSE	R (K)	Bias (K)	RMSE	R (K)	Bias (K)	RMSE
T_{bh} Constant τ_p	0.76	–0.85	5.48	0.75	–2.04	6.10	0.75	–0.03	5.48
T_{bh} Varying τ_p	0.78	–1.45	7.06	0.78	–2.58	7.53	0.78	–0.45	6.45
T_{bv} Constant τ_p	0.76	2.27	5.45	0.76	1.97	5.63	0.76	3.26	5.98
T_{bv} Varying τ_p	0.74	1.93	6.61	0.74	1.66	6.73	0.75	3.01	6.71

5.2. Uncertainties in the Model Simulations

5.2.1. Uncertainties in the Hydrology Model Simulation

To better simulate SM dynamics in the northern permafrost region, a reliable soil parameterization that can apply to a wide range of organic soils is needed. Depending on the degree of decomposition, organic/peaty soils can have quite different water-retention characteristics and hydraulic conductivity (Verry et al., 2011). However, most current land models do not account for this variability; these models generally only account for the influence of SOC content on the estimated soil hydraulic parameters, or they use a single "peat" category to represent the broad range of organic soils in the Arctic (e.g., De Lannoy et al., 2014; Guimberteau et al., 2018; Rawlins et al., 2019). Soil bulk density decreases exponentially with SOC concentration, and the total SOC content, as the product of bulk density and SOC concentration, peaks at intermediate SOC concentration (Hossain et al., 2015). Thus, the total SOC content or SOC density is generally not a good proxy for the soil organic fraction as used in the land models. In this study, we introduced a soil parameterization that uses the "fiber content" to link the SOC decomposition state with variations in the organic soil hydraulic properties. The fiber content is empirically related to SOC concentration calibrated using the USDA-NCCS soil database covering the full range of organic soils (Chen et al., 2019). SOC concentration or bulk density data are available from several global soil data sets including the SoilGrids and HWSD (the Harmonized World Soil Database; Poggio et al., 2021; Tifafi et al., 2018), which makes this parameterization potentially useful for regional applications despite large uncertainties in those data sets. However, additional soil characteristics data are needed to test this parameterization for different organic soils. In our study, we did not discuss the model uncertainty associated with the uncertainties in the soil parameterization; rather, we characterize this uncertainty by varying the SOM profile in the model calibration experiments.

In addition, a lack of reliable in situ data including SM and ET introduces challenges to the model calibration and validation, and further understanding of the processes controlling SM dynamics in the Arctic region is needed. A number of field studies have pointed out that lateral water transfer can play an important role in regulating soil drainage during the spring thaw period (e.g., Quinton et al., 2000; Woo & Marsh, 2005), which is not considered by the current model. This may add additional uncertainty to the model characterization of the spring "drydown" process. There are a number of issues associated with eddy covariance measurement methods in the Arctic region and significant data loss is generally expected in extreme conditions (Euskirchen, Edgar, et al., 2017). Therefore, the quality of the final flux products used for the model calibration and validation is subject to the accuracy of the underlying gap-filling methods. It is also a challenge to measure the heat fluxes during the winter time (Euskirchen, Edgar, et al., 2017), when snow sublimation and deposition can be important to determine the snow mass and significantly affect the soil thermal regime (Strasser et al., 2008; Yi et al., 2019). High-quality SM data are also lacking in the northern permafrost region. The lack of a reliable and generic calibration function for organic soils introduces uncertainty to in situ SM data in the Arctic region (Bircher et al., 2016a). The location of the soil sensor can change dramatically due to active soil frost heave in the permafrost region (Romanovsky et al., 2008), which can result in discontinuities in the SM measurements as indicated by the Imnavait Creek site data.

5.2.2. Uncertainties in the Tb Simulation

As can be seen from the above tau-omega model calibration, there are substantial uncertainties in the VOD and roughness parameters. Due to a compensation effect of VOD and roughness parameters on the Tb simulation, our calibration experiments selected three sets of VOD and roughness values (Tables 6 and 7). There is generally a

lack of data on changes in the vegetation water content and surface roughness height in Arctic tundra. Therefore, we cannot tell which is the best solution. Using a mean VOD value of 0.35, the estimates of vegetation water content range from ~1.5 to 2.0 kg/m^2 during the thaw season, while a recent study based on in situ data and Landsat imagery provides an estimate of aboveground biomass of ~0.81–1.18 kg/m^2 for shrub tundra in the Alaska North Slope (Berner et al., 2018). Previous studies provide estimates of relative water content for leaves and shoots ranging from ~60% to more than 150% (Huang et al., 2019; Saura-Mas & Lloret, 2007). Therefore, the above vegetation water content estimates are at the high-end of the realistic range. However, multiple or volume scattering may also occur within the surface organic or litter layer, which can increase the surface emissions. The tau-omega model does not account for the above scattering processes, and thus the optimization may give a higher estimate of VOD to compensate for the above effects.

Previous studies also showed that higher values of the roughness parameter are associated with drier soil conditions (De Lannoy et al., 2013; Neelam et al., 2020); however, including a moisture-dependent function for this parameter did not produce significant improvements in the model simulations. On the other hand, the presence of surface litter and undecomposed organic materials in the surface organic layer may result in increasing attenuation of soil emissions or volumetric scattering (Kerr et al., 2012; Zweivack & Berg, 2019). Using the zero-order tau-omega model may result in large uncertainties in this condition, which mainly represent surface scattering. The inconsistency between the model PR simulations and SMAP observations during the later thaw season may be also partly due to the above uncertainty; during this period, surface soil is relatively wet due to precipitation inputs and lower evaporative demand, while the L-band PR shows reduced sensitivity to surface SM changes. Finally, uncertainty in the soil dielectric constant also contributes to uncertainties in the tau-omega model simulations. There is currently no mature soil dielectric model for organic soils (Bircher et al., 2016b; Park et al., 2019). A major challenge in dielectric modeling is to characterize the bound-water fraction with SM changes for different organic soil types.

6. Conclusions

In this study, we combined data analysis and process-based modeling to better understand the links between surface soil organic carbon properties and SM dynamics in Arctic tundra underlain by continuous permafrost. Our analysis using both in situ SM and SMAP L-band brightness temperature data confirmed the important control of surface organic soil on SM dynamics in Arctic tundra. Surface soil generally dries faster in areas with higher surface SOC concentration. Our analysis indicated that the L-band PR was sensitive to the tundra surface SM dynamics, especially during the early thaw period, and contains useful information on surface organic soil properties including SOC concentration and bulk density. Our modeling experiments also supported the above conclusion. Through using a coupled model with improved soil parameterization and dielectric modeling for organic soils characteristic of tundra, we demonstrated that highly organic tundra soils (SOCC > ~34.8%) with a higher amount of fibrous organic materials (or fiber content) generally showed larger decreases in the L-band PR with soil drydown during the early thaw period. This is likely because highly organic soils drain water more easily (both vertically and laterally), and a larger amount of water can be discharged or lost (through evapotranspiration) in those soils, relative to soils with low SOC concentration (SOCC < ~17.4%). However, our modeling experiments also demonstrated that changes in vegetation water content and surface roughness throughout the thaw season may introduce additional uncertainty to the above analysis of L-band PR sensitivity to surface SM and SOC conditions. To future improve modeling of surface SM dynamics and organic carbon distribution using L-band sensing, a better understanding of the temporal and spatial variability of the above two parameters in the Arctic region is critical. Our study indicates new capabilities for pan-Arctic mapping and monitoring of organic soil properties using low frequency satellite microwave measurements, which may allow for improved Earth system model projections of regional water-carbon-energy exchanges and linkages and feedbacks to climate change in the Arctic.

Appendix A: Soil Dielectric Modeling

Organic soils exhibit different dielectric properties from mineral soils (Bircher et al., 2016a), which should be accounted for when estimating soil dielectric constant (ε) under variable SM levels or vice versa. Currently, robust soil dielectric models that can be applied to soils with a wide range of SOM conditions are lacking. Here,

we used the dielectric mixing model developed by Park et al. (2017) to calculate the effective ε of the multi-phase soil based on the arithmetic average of ε values of soil components:

$$\varepsilon = (1-\theta_s)\times\varepsilon_{soil} + \theta\times\varepsilon_{water} + (\theta_s-\theta)\times\varepsilon_{air} \tag{A1}$$

$$\varepsilon_{water} = (\theta_{liq}\cdot\upsilon_{bound})\times\varepsilon_{bound} + (\theta_{liq}\cdot\upsilon_{free})\times\varepsilon_{free} + \theta_{ice}\times\varepsilon_{ice} \tag{A2}$$

where θ_s, θ_{ice}, and θ_{liq} represent soil porosity, ice and liquid water content (cm^3/cm^3), respectively, with $\theta = \theta_{ice} + \theta_{liq}$. υ_{free} and υ_{bound} are the fractions of free and bound liquid water, with $\upsilon_{free} + \upsilon_{bound} = 1$. ε_{soil}, ε_{air}, ε_{ice}, ε_{bound}, ε_{free} are the dielectric constants of soil solids (mineral or organic), air, ice, bound and free water, respectively, which can be found in Park et al. (2017). Park's dielectric model was developed to be integrated with land surface models (LSMs), as all information can be obtained through the LSM or hydrology model. Previous studies showed that Park's model provides favorable performance for both mineral soils (Park et al., 2017) and organic soils with different SOM concentrations (Park et al., 2019).

A key parameter in dielectric modeling is the bound-water fraction. In Park et al. (2017), the following equation is used to determine the free and bound-water fractions in soil:

$$\begin{aligned} \upsilon_{bound} &= 1, && if\ \theta < \theta_{vt} \\ \upsilon_{bound} &= \frac{\varnothing-\theta}{\varnothing-\theta_{vt}}, && if\ \theta \geq \theta_{vt} \end{aligned} \tag{A3}$$

where θ_{vt} is the point at which water switches from bound to free state. In Park et al. (2017, 2019), the SM at wilting point was used as a proxy for θ_{vt}. In our soil parameterization, the wilting point of highly organic soils (SOM > 0.8) was very low, which was consistent with field data (Verry et al., 2011). However, previous studies suggest soils with higher organic matter generally contain a high proportion of bound water due to the strong ability of humus materials to absorb water. Therefore, we used the following equation as in Park et al. (2019) and Jin et al. (2013) to estimate the transitional point (θ_{vt}):

$$\theta_{vt} = 0.02982 + 0.00786\times(\mathrm{SOM}\times 100) + 0.00089\times clay\% \tag{A4}$$

where $clay\%$ is percentage of clay (volumetric) in soil. Equation A4 gives a very high estimate of θ_{vt} for highly organic soil, and therefore we limit this value to 0.4. Compared with using the wilting point, using θ_{vt} derived from Equation A4 gives a closer estimate of ε for highly organic soils at 70 MHz (Figure S3 in Supporting Information S1) as the data presented in Bircher et al. (2016a). A more detailed comparison of Park's model with other dielectric models is provided in Supporting Information S1.

Appendix B: Evapotranspiration Modeling Improvements in the PWBM Model

In this study, we revised the ET scheme in the PWBM model using the following steps. We first revised the potential ET (PET) calculation. In the original model, PET calculation was based on the Hamon method, which requires minimal meteorology data, but has relatively lower accuracy than radiation-based methods for PET estimation such as the Makkink model (Lang et al., 2017; Xu & Chen, 2005). Therefore, we used the Makkink method to estimate PET (mm/day; Xu & Chen, 2005):

$$PET = 0.61\times\frac{\Delta}{\Delta+\gamma}\times\frac{R_s}{L_v} - 0.012 \tag{A5}$$

where R_s is the downward solar radiation (MJ/m^2/day), Δ is the slope of the saturation water vapor-temperature curve at the given air temperature, L_v is the latent heat of vaporization (2.45 MJ/m^2), and γ is the psychrometric constant.

We then modeled soil evaporation and plant transpiration separately. Soil evaporation was limited by the soil water in the top two surface layers (0–5.5 cm), while the plants can uptake water from the entire root zone. The root zone was defined by the rooting depth (Jackson et al., 1996) and can change dynamically based on the soil water freeze/thaw status within the rooting depth as:

$$\mathrm{ET}_{soil,i=1,2} = \mathrm{PET}\times(1-f_{veg})\times f(\mathrm{SM}_i) \tag{A6}$$

$$\mathrm{ET}_{plants,i=1,n} = \mathrm{PET} \times f_{veg} \times f(\mathrm{SM}_i) \times \frac{rootfrac_i \times f_{liq,i}}{\sum_{ilayer=1}^{n} rootfrac_{ilayer} \times f_{liq,ilayer}} \quad \text{(A7)}$$

The last term in Equation A7 accounts for the dynamic changes in the root zone with soil liquid water content (f_{liq}), and $rootfrac$ is the root fraction within each soil layer. f(SM) is a step function of SM, which was set to 0 below the wilting point, 1 above field capacity, and scaled linearly between the two SM values. The MODIS 16-day NDVI (normalized difference vegetation index) observational record (MOD13A2) was used to estimate the vegetation coverage (f_{veg}) using a linear relationship (Carlson & Ripley, 1997).

Finally, the snow sublimation rate (mm/day) was estimated using an empirical equation valid for the conditions of medium roughness, stable stratification and a wide range of wind speeds (Strasser et al., 2008):

$$Subl = f \times (32.82 \times (0.18 + 0.098 \times Windsp) \times VPD \times dt)/L_s \quad \text{(A8)}$$

where $Windsp$ and VPD are wind speed (m/s) and vapor pressure deficit at the snow surface (hpa), respectively, dt is the modeling time step (s), L_s is the sublimation heat of snow (2.838 kJ/kg), and f is an empirical scaling factor that can be adjusted locally.

Data Availability Statement

MAP and MODIS data are available from NASA Earth-data (https://earthdata.nasa.gov/). SoilSCAPE data is available from https://soilscape.usc.edu. Daymet surface meteorology was downloaded from https://daymet.ornl.gov/. SNOTEL data was obtained online from https://www.wcc.nrcs.usda.gov/snow/. Data at the Imnavait Creek EC tower sites were downloaded from http://aon.iab.uaf.edu/data.

Acknowledgments
Data at the Imnavait Creek EC tower sites have been collected through grants from the Arctic Observatory Program of the National Science Foundation (Grant Nos. 1936752, 1503912, 1107892). The study was supported by the NASA ABOVE (Arctic Boreal Vulnerability Experiment; 80NSSC19M0114) and Terrestrial Hydrology program (80NSSC21K1340, 80NSSC19K0649). Part of the work was conducted at Jet Propulsion Laboratory, California Institute of Technology, under a contract with NASA

References

Andresen, C. G., Lawrence, D. M., Wilson, C. J., McGuire, A. D., Koven, C., Schaefer, K., et al. (2020). Soil moisture and hydrology projections of the permafrost region—A model intercomparison. *The Cryosphere*, *14*(2), 445–459. https://doi.org/10.5194/tc-14-445-2020

Bakian-Dogaheh, K., Chen, R. H., Moghaddam, M., Yi, Y., & Tabatabaeenejad, A. (2020). *ABoVE: Active layer soil characterization of permafrost sites, northern Alaska, 2018*. ORNL DAAC. https://doi.org/10.3334/ORNLDAAC/1759

Bechtold, M., De Lannoy, G. J. M., Koster, R. D., Reichle, R. H., Mahanama, S. P., Bleuten, W., et al. (2019). PEAT-CLSM: A specific treatment of peatland hydrology in the NASA Catchment land surface model. *Journal of Advances in Modeling Earth Systems*, *11*, 2130–2162. https://doi.org/10.1029/2018MS001574

Bechtold, M., De Lannoy, G. J. M., Reichle, R. H., Roose, D., Balliston, N., Burdun, I., et al. (2020). Improved groundwater table and L-band brightness temperature estimates for Northern Hemisphere peatlands using new model physics and SMOS observations in a global data assimilation framework. *Remote Sensing of Environment*, *246*, 111805. https://doi.org/10.1016/j.rse.2020.111805

Berner, L. T., Jantz, P., Tape, K. D., & Goetz, S. J. (2018). Tundra plant above-ground biomass and shrub dominance mapped across the North Slope of Alaska. *Environmental Research Letters*, *13*(3), 035002. https://doi.org/10.1088/1748-9326/aaaa9a

Bircher, S., Andreasen, M., Vuollet, J., Vehviläinen, J., Rautiainen, K., Jonard, F., et al. (2016a). Soil moisture sensor calibration for organic soil surface layers. *Geoscientific Instrumentation, Methods and Data Systems*, *5*(1), 109–125. https://doi.org/10.5194/gi-5-109-2016

Bircher, S., Demontoux, F., Razafindratsima, S., Zakharova, E., Drusch, M., Wigneron, J.-P., & Kerr, Y. (2016b). L-band relative permittivity of organic soil surface layers—A new dataset of resonant cavity measurements and model evaluation. *Remote Sensing*, *8*(12), 1024. https://doi.org/10.3390/rs8121024

Biskaborn, B. K., Smith, S. L., Noetzli, J., Matthes, H., Vieira, G., Streletskiy, D. A., et al. (2019). Permafrost is warming at a global scale. *Nature Communications*, *10*(1), 264. https://doi.org/10.1038/s41467-018-08240-4

Boelter, D. H. (1969). Physical properties of peats as related to degree of decomposition. *Soil Science Society of America Proceedings*, *33*(4), 606–609. https://doi.org/10.2136/sssaj1969.03615995003300040033x

Burke, E. J., Gurney, R. J., Simmonds, L. P., & O'Neill, P. E. (1998). Using a modeling approach to predict soil hydraulic properties from passive microwave measurements. *IEEE Transactions on Geoscience and Remote Sensing*, *36*(2), 454–462. https://doi.org/10.1109/36.662729

Camillo, P., O'Neill, P., & Gurney, R. (1986). Estimating soil hydraulic parameters using passive microwave data. *IEEE Transactions on Geoscience and Remote Sensing*, *24*(6), 930–936. https://doi.org/10.1109/TGRS.1986.289708

Campbell, G. S. (1974). A simple method for determining unsaturated conductivity from moisture retention data. *Soil Science*, *117*(6), 311–314. https://doi.org/10.1097/00010694-197406000-00001

Carlson, T. N., & Ripley, D. A. (1997). On the relation between NDVI, fractional vegetation cover, and leaf area index. *Remote Sensing of Environment*, *62*(3), 241–252. https://doi.org/10.1016/S0034-4257(97)00104-1

Chan, S., Bindlish, R., Hunt, R., Jackson, T., & Kimball, J. (2013). *Soil moisture active passive (SMAP) ancillary data report: Vegetation water content*. Jet Propulsion Laboratory.

Chan, S. K., Bindlish, R., O'Neill, P. E., Njoku, E., Jackson, T., Colliander, A., et al. (2016). Assessment of the SMAP passive soil moisture product. *IEEE Transactions on Geoscience and Remote Sensing*, *54*(8), 4994–5007. https://doi.org/10.1109/TGRS.2016.2561938

Chaubell, J., Chan, S., Dunbar, R. S., Peng, J., & Yueh, S. (2020). *SMAP enhanced L1C radiometer Half-Orbit 9 km EASE-grid brightness temperatures, Version 3*. NASA National Snow and Ice Data Center Distributed Active Archive Center. https://doi.org/10.5067/XB8K63YM4U8O

Chen, R. H., Bakian-Dogaheh, K., Tabatabaeenejad, A., & Moghaddam, M. (2019). Modeling and retrieving soil moisture and organic matter profiles in the active layer of permafrost soils from P-band radar observations. Paper presented at IGARSS 2019—2019 IEEE International Geoscience and Remote Sensing Symposium. IEEE. https://doi.org/10.1109/IGARSS.2019.8899802

Chen, R. H., Michaelides, R. J., Sullivan, T. D., Parsekian, A. D., Zebker, H. A., Moghaddam, M., & Schaefer, K. M. (2020). Joint retrieval of soil moisture and permafrost active layer Thickness using L-band insar and P-band Polsar. Paper presented at IGARSS 2020—2020 IEEE International Geoscience and Remote Sensing Symposium. IEEE. https://doi.org/10.1109/IGARSS39084.2020.9324660

Colliander, A., Cosh, M. H., Kelly, V. R., Kraatz, S., Bourgeau-Chavez, L., Siqueira, P., et al. (2020). SMAP detects soil moisture under temperate forest Canopies. *Geophysical Research Letters*, *47*, e2020GL089697. https://doi.org/10.1029/2020GL089697

Connon, R., Devoie, É., Hayashi, M., Veness, T., & Quinton, W. (2018). The influence of shallow taliks on permafrost thaw and active layer dynamics in Subarctic Canada. *Journal of Geophysical Research: Earth Surface*, *123*, 281–297. https://doi.org/10.1002/2017JF004469

De Lannoy, G. J. M., Koster, R. D., Reichle, R. H., Mahanama, S. P. P., & Liu, Q. (2014). An updated treatment of soil texture and associated hydraulic properties in a global land modeling system. *Journal of Advances in Modeling Earth Systems*, *6*, 957–979. https://doi.org/10.1002/2014MS000330

De Lannoy, G. J. M., Reichle, R. H., & Pauwels, V. R. N. (2013). Global calibration of the GEOS-5 L-band microwave radiative transfer model over nonfrozen land using SMOS observations. *Journal of Hydrometeorology*, *14*(3), 765–785. https://doi.org/10.1175/JHM-D-12-092.1

Decharme, B., Brun, E., Boone, A., Delire, C., Le Moigne, P., & Morin, S. (2016). Impacts of snow and organic soils parameterization on northern Eurasian soil temperature profiles simulated by the ISBA land surface model. *The Cryosphere*, *10*(2), 853–877. https://doi.org/10.5194/tc-10-853-2016

Derksen, C., Xu, X., Scott Dunbar, R., Colliander, A., Kim, Y., Kimball, J. S., et al. (2017). Retrieving landscape freeze/thaw state from Soil Moisture Active Passive (SMAP) radar and radiometer measurements. *Remote Sensing of Environment*, *194*, 48–62. https://doi.org/10.1016/j.rse.2017.03.007

Escorihuela, M. J., Chanzy, A., Wigneron, J. P., & Kerr, Y. H. (2010). Effective soil moisture sampling depth of L-band radiometry: A case study. *Remote Sensing of Environment*, *114*(5), 995–1001. https://doi.org/10.1016/j.rse.2009.12.011

Euskirchen, E. S., Bret-Harte, M. S., Shaver, G. R., Edgar, C. W., & Romanovsky, V. E. (2017). Long-term release of carbon dioxide from arctic tundra ecosystems in Alaska. *Ecosystems*, *20*(5), 960–974. https://doi.org/10.1007/s10021-016-0085-9

Euskirchen, E. S., Edgar, C. W., Syndonia Bret-Harte, M., Kade, A., Zimov, N., & Zimov, S. (2017). Interannual and seasonal patterns of carbon dioxide, water, and energy fluxes from ecotonal and thermokarst-impacted ecosystems on carbon-rich permafrost soils in Northeastern Siberia: Siberian CO_2, water, and energy fluxes. *Journal of Geophysical Research: Biogeosciences*, *122*, 2651–2668. https://doi.org/10.1002/2017JG004070

Gao, Y., Walker, J. P., Ye, N., Panciera, R., Monerris, A., Ryu, D., et al. (2018). Evaluation of the tau-omega model for passive microwave soil moisture retrieval using SMAPEx datasets. *IEEE Journal of Selected Topics in Applied Earth Observations and Remote Sensing*, *11*(3), 888–895. https://doi.org/10.1109/JSTARS.2018.2796546

Gherboudj, I., Magagi, R., Goita, K., Berg, A. A., Toth, B., & Walker, A. (2012). Validation of SMOS data over agricultural and boreal forest areas in Canada. *IEEE Transactions on Geoscience and Remote Sensing*, *50*(5), 1623–1635. https://doi.org/10.1109/TGRS.2012.2188532

Goffe, W. L., Ferrier, G. D., & Rogers, J. (1994). Global optimization of statistical functions with simulated annealing. *Journal of Econometrics*, *60*(1–2), 65–99. https://doi.org/10.1016/0304-4076(94)90038-8

Guimberteau, M., Zhu, D., Maignan, F., Huang, Y., Yue, C., Dantec-Nédélec, S., et al. (2018). ORCHIDEE-MICT (v8.4.1), a land surface model for the high latitudes: Model description and validation. *Geoscientific Model Development*, *11*(1), 121–163. https://doi.org/10.5194/gmd-11-121-2018

Hengl, T., Mendes de Jesus, J., Heuvelink, G. B. M., Ruiperez Gonzalez, M., Kilibarda, M., Blagotić, A., et al. (2017). SoilGrids250m: Global gridded soil information based on machine learning. *PLoS One*, *12*(2), e0169748. https://doi.org/10.1371/journal.pone.0169748

Hossain, M. F., Chen, W., & Zhang, Y. (2015). Bulk density of mineral and organic soils in the Canada's arctic and sub-arctic. *Information Processing in Agriculture*, *2*(3–4), 183–190. https://doi.org/10.1016/j.inpa.2015.09.001

Huang, W., Ratkowsky, D., Hui, C., Wang, P., Su, J., & Shi, P. (2019). Leaf fresh weight versus dry weight: Which is better for describing the scaling relationship between leaf biomass and leaf area for broad-Leaved plants? *Forests*, *10*(3), 256. https://doi.org/10.3390/f10030256

Hugelius, G., Loisel, J., Chadburn, S., Jackson, R. B., Jones, M., MacDonald, G., et al. (2020). Large stocks of peatland carbon and nitrogen are vulnerable to permafrost thaw. *Proceedings of the National Academy of Sciences of the United States of America*, *117*(34), 20438–20446. https://doi.org/10.1073/pnas.1916387117

Jackson, R. B., Canadell, J., Ehleringer, J. R., Mooney, H. A., Sala, O. E., & Schulze, E. D. (1996). A global analysis of root distributions for terrestrial biomes. *Oecologia*, *108*(3), 389–411. https://doi.org/10.1007/BF00333714

Jin, S., Yang, L., Danielson, P., Homer, C., Fry, J., & Xian, G. (2013). A comprehensive change detection method for updating the National Land Cover Database to circa 2011. *Remote Sensing of Environment*, *132*, 159–175. https://doi.org/10.1016/j.rse.2013.01.012

Jonard, F., Bircher, S., Demontoux, F., Weihermüller, L., Razafindratsima, S., Wigneron, J.-P., & Vereecken, H. (2018). Passive L-band microwave remote sensing of organic soil surface layers: A tower-based experiment. *Remote Sensing*, *10*(2), 304. https://doi.org/10.3390/rs10020304

Kerr, Y. H., Waldteufel, P., Richaume, P., Wigneron, J. P., Ferrazzoli, P., Mahmoodi, A., et al. (2012). The SMOS soil moisture retrieval algorithm. *IEEE Transactions on Geoscience and Remote Sensing*, *50*(5), 1384–1403. https://doi.org/10.1109/TGRS.2012.2184548

Kurc, S. A., & Small, E. E. (2004). Dynamics of evapotranspiration in semiarid grassland and shrubland ecosystems during the summer monsoon season, central New Mexico. *Water Resources Research*, *40*, W09305. https://doi.org/10.1029/2004WR003068

Kurylyk, B. L., Hayashi, M., Quinton, W. L., McKenzie, J. M., & Voss, C. I. (2016). Influence of vertical and lateral heat transfer on permafrost thaw, peatland landscape transition, and groundwater flow: Permafrost thaw, landscape change, and groundwater flow. *Water Resources Research*, *52*, 1286–1305. https://doi.org/10.1002/2015WR018057

Lang, D., Zheng, J., Shi, J., Liao, F., Ma, X., Wang, W., et al. (2017). A Comparative study of potential evapotranspiration estimation by eight methods with FAO Penman-Monteith method in Southwestern China. *Water*, *9*(10), 734. https://doi.org/10.3390/w9100734

Lawrence, D. M., & Slater, A. G. (2008). Incorporating organic soil into a global climate model. *Climate Dynamics*, *30*(2–3), 145–160. https://doi.org/10.1007/s00382-007-0278-1

Letts, M. G., Roulet, N. T., Comer, N. T., Skarupa, M. R., & Verseghy, D. L. (2000). Parametrization of peatland hydraulic properties for the Canadian land surface scheme. *Atmosphere-Ocean*, *38*(1), 141–160. https://doi.org/10.1080/07055900.2000.9649643

Liljedahl, A. K., Boike, J., Daanen, R. P., Fedorov, A. N., Frost, G. V., Grosse, G., et al. (2016). Pan-Arctic ice-wedge degradation in warming permafrost and its influence on tundra hydrology. *Nature Geoscience*, *9*, 8. https://doi.org/10.1038/ngeo2674

Mattikalli, N. M., Engman, E. T., Jackson, T. J., & Ahuja, L. R. (1998). Microwave remote sensing of temporal variations of brightness temperature and near-surface soil water content during a watershed-scale field experiment, and its application to the estimation of soil physical properties. *Water Resources Research*, *34*, 2289–2299. https://doi.org/10.1029/98WR00553

McColl, K. A., He, Q., Lu, H., & Entekhabi, D. (2019). Short-term and long-term surface soil moisture memory time scales are spatially anticorrelated at global scales. *Journal of Hydrometeorology*, *20*(6), 1165–1182. https://doi.org/10.1175/JHM-D-18-0141.1

McColl, K. A., Wang, W., Peng, B., Akbar, R., Short Gianotti, D. J., Lu, H., et al. (2017). Global characterization of surface soil moisture drydowns. *Geophysical Research Letters*, *44*, 3682–3690. https://doi.org/10.1002/2017GL072819

Mironov, V. L., Kerr, Y. H., Kosolapova, L. G., Savin, I. V., & Muzalevskiy, K. V. (2015). A temperature-dependent dielectric model for thawed and frozen organic soil at 1.4 GHz. *IEEE Journal of Selected Topics in Applied Earth Observations and Remote Sensing*, *8*(9), 4470–4477. https://doi.org/10.1109/JSTARS.2015.2442295

Mironov, V. L., Kosolapova, L. G., & Fomin, S. V. (2009). Physically and mineralogically based spectroscopic dielectric model for moist soils. *IEEE Transactions on Geoscience and Remote Sensing*, *47*(7), 2059–2070. https://doi.org/10.1109/TGRS.2008.2011631

Mishra, U., Hugelius, G., Shelef, E., Yang, Y., Strauss, J., Lupachev, A., et al. (2021). Spatial heterogeneity and environmental predictors of permafrost region soil organic carbon stocks. *Science Advances*, *7*(9). eaaz5236. https://doi.org/10.1126/sciadv.aaz5236

Mishra, U., & Riley, W. J. (2015). Scaling impacts on environmental controls and spatial heterogeneity of soil organic carbon stocks. *Biogeosciences*, *12*(13), 3993–4004. https://doi.org/10.5194/bg-12-3993-2015

Neelam, M., Colliander, A., Mohanty, B. P., Cosh, M. H., Misra, S., & Jackson, T. J. (2020). Multiscale surface roughness for improved soil moisture estimation. *IEEE Transactions on Geoscience and Remote Sensing*, *58*(8), 5264–5276. https://doi.org/10.1109/TGRS.2019.2961008

O'Connor, M. T., Cardenas, M. B., Ferencz, S. B., Wu, Y., Neilson, B. T., Chen, J., & Kling, G. W. (2020). Empirical models for predicting water and heat flow properties of permafrost soils. *Geophysical Research Letters*, *47*, e2020GL087646. https://doi.org/10.1029/2020GL087646

Paloscia, S., Pampaloni, P., & Santi, E. (2018). Radiometric microwave indices for remote sensing of land surfaces. *Remote Sensing*, *10*(12), 1859. https://doi.org/10.3390/rs10121859

Paquin, J.-P., & Sushama, L. (2015). On the Arctic near-surface permafrost and climate sensitivities to soil and snow model formulations in climate models. *Climate Dynamics*, *44*(1–2), 203–228. https://doi.org/10.1007/s00382-014-2185-6

Park, C.-H., Behrendt, A., LeDrew, E., & Wulfmeyer, V. (2017). New approach for calculating the effective dielectric constant of the moist soil for microwaves. *Remote Sensing*, *9*(7), 732. https://doi.org/10.3390/rs9070732

Park, C.-H., Montzka, C., Jagdhuber, T., Jonard, F., De Lannoy, G., Hong, J., et al. (2019). A dielectric mixing model accounting for soil organic matter. *Vadose Zone Journal*, *18*(1), 190036. https://doi.org/10.2136/vzj2019.04.0036

Poggio, L., Sousa, L. M., Batjes, N. H., Heuvelink, G. B. M., Kempen, B., Ribeiro, E., & Rossiter, D. (2021). SoilGrids 2.0: Producing soil information for the globe with quantified spatial uncertainty. *SOIL*, *7*(1), 217–240. https://doi.org/10.5194/soil-7-217-2021

Pribyl, D. W. (2010). A critical review of the conventional SOC to SOM conversion factor. *Geoderma*, *156*(3–4), 75–83. https://doi.org/10.1016/j.geoderma.2010.02.003

Quinton, W. L., Gray, D. M., & Marsh, P. (2000). Subsurface drainage from hummock-covered hillslopes in the Arctic tundra. *Journal of Hydrology*, *237*(1–2), 113–125. https://doi.org/10.1016/S0022-1694(00)00304-8

Quinton, W. L., & Marsh, P. (1998). The influence of mineral Earth hummocks on subsurface drainage in the continuous permafrost zone. *Permafrost and Periglacial Processes*, *9*(3), 213–228. https://doi.org/10.1002/(SICI)1099-1530(199807/09)9:3<213::AID-PPP285>3.0.CO;2-E

Rawlins, M. A., Cai, L., Stuefer, S. L., & Nicolsky, D. (2019). Changing characteristics of runoff and freshwater export from watersheds draining northern Alaska. *The Cryosphere*, *13*(12), 3337–3352. https://doi.org/10.5194/tc-13-3337-2019

Rawlins, M. A., Nicolsky, D. J., McDonald, K. C., & Romanovsky, V. E. (2013). Simulating soil freeze/thaw dynamics with an improved pan-Arctic water balance model. *Journal of Advances in Modeling Earth Systems*, *5*, 659–675. https://doi.org/10.1002/jame.20045

Romanovsky, V. E., Marchenko, S. S., Daanen, R., Sergeev, D. O., & Walker, D. A. (2008). *Soil climate and frost heave along the permafrost* (Vol. 6). Ecological North American Arctic Transect.

Rondinelli, W. J., Hornbuckle, B. K., Patton, J. C., Cosh, M. H., Walker, V. A., Carr, B. D., & Logsdon, S. D. (2015). Different rates of soil drying after rainfall are observed by the SMOS satellite and the south Fork in situ soil moisture network. *Journal of Hydrometeorology*, *16*(2), 889–903. https://doi.org/10.1175/JHM-D-14-0137.1

Roy, A., Toose, P., Williamson, M., Rowlandson, T., Derksen, C., Royer, A., et al. (2017). Response of L-Band brightness temperatures to freeze/thaw and snow dynamics in a prairie environment from ground-based radiometer measurements. *Remote Sensing of Environment*, *191*, 67–80. https://doi.org/10.1016/j.rse.2017.01.017

Santanello, J. A., Peters-Lidard, C. D., Garcia, M. E., Mocko, D. M., Tischler, M. A., Moran, M. S., & Thoma, D. P. (2007). Using remotely-sensed estimates of soil moisture to infer soil texture and hydraulic properties across a semi-arid watershed. *Remote Sensing of Environment*, *110*(1), 79–97. https://doi.org/10.1016/j.rse.2007.02.007

Saura-Mas, S., & Lloret, F. (2007). Leaf and shoot water content and leaf dry matter content of Mediterranean woody species with different post-fire regenerative strategies. *Annals of Botany*, *99*(3), 545–554. https://doi.org/10.1093/aob/mcl284

Schmugge, T. J. (1983). Remote sensing of soil moisture: Recent advances. *IEEE Transactions on Geoscience and Remote Sensing*, *21*(3), 336–344. https://doi.org/10.1109/TGRS.1983.350563

Schwank, M., Naderpour, R., & Mätzler, C. (2018). Tau-omega"- and two-stream emission models used for passive L-band retrievals: Application to close-range measurements over a forest. *Remote Sensing*, *10*(12), 1868. https://doi.org/10.3390/rs10121868

Shellito, P. J., Small, E. E., Colliander, A., Bindlish, R., Cosh, M. H., Berg, A. A., et al. (2016). SMAP soil moisture drying more rapid than observed in situ following rainfall events. *Geophysical Research Letters*, *43*, 8068–8075. https://doi.org/10.1002/2016GL069946

Shi, X., Thornton, P. E., Ricciuto, D. M., Hanson, P. J., Mao, J., Sebestyen, S. D., et al. (2015). Representing Northern Peatland microtopography and hydrology within the community land mode. *Biogeosciences Discussions*, *12*(4), 3381–3418.

Strasser, U., Bernhardt, M., Weber, M., Liston, G. E., & Mauser, W. (2008). Is snow sublimation important in the alpine water balance? *The Cryosphere*, *2*, 53–66. https://doi.org/10.5194/tc-2-53-2008

Thornton, M. M., Shrestha, R., Wei, Y., Thornton, P. E., Kao, S., & Wilson, B. E. (2020). *Daymet: Daily surface weather data on a 1-km grid for North America, Version 4*. ORNL DAAC. https://doi.org/10.3334/ORNLDAAC/1840

Tifafi, M., Guenet, B., & Hatté, C. (2018). Large differences in global and regional total soil carbon stock estimates based on SoilGrids, HWSD, and NCSCD: Intercomparison and evaluation based on field data from USA, England, Wales, and France. *Global Biogeochemical Cycles*, *32*, 42–56. https://doi.org/10.1002/2017GB005678

Verry, E., Boelter, D., Päivänen, J., Nichols, D., Malterer, T., & Gafni, A. (2011). Physical properties of organic soils. In K.Brooks (Ed.), *Peatland Biogeochemistry and watershed hydrology at the Marcell experimental forest* (pp. 135–176). CRC Press. https://doi.org/10.1201/b10708-6

Vonk, J. E., Tank, S. E., & Walvoord, M. A. (2019). Integrating hydrology and biogeochemistry across frozen landscapes. *Nature Communications*, *10*(1), 5377. https://doi.org/10.1038/s41467-019-13361-5

Wigneron, J.-P., Chanzy, A., Rosnay, P., Rudiger, C., & Calvet, J.-C. (2008). Estimating the effective soil temperature at L-band as a function of soil properties. *IEEE Transactions on Geoscience and Remote Sensing*, *46*(3), 797–807. https://doi.org/10.1109/TGRS.2007.914806

Woo, M.-K., & Marsh, P. (2005). Snow, frozen soils and permafrost hydrology in Canada, 1999–2002. *Hydrological Processes*, *19*(1), 215–229. https://doi.org/10.1002/hyp.5772

Wrona, E., Rowlandson, T. L., Nambiar, M., Berg, A. A., Colliander, A., & Marsh, P. (2017). Validation of the soil moisture active passive (SMAP) satellite soil moisture retrieval in an arctic tundra environment: Validation of SMAP in arctic tundra. *Geophysical Research Letters*, *44*, 4152–4158. https://doi.org/10.1002/2017GL072946

Xu, C.-Y., & Chen, D. (2005). Comparison of seven models for estimation of evapotranspiration and groundwater recharge using lysimeter measurement data in Germany. *Hydrological Processes*, *19*(18), 3717–3734. https://doi.org/10.1002/hyp.5853

Yi, Y., Kimball, J. S., Chen, R. H., Moghaddam, M., & Miller, C. E. (2019). Sensitivity of active-layer freezing process to snow cover in Arctic Alaska. *The Cryosphere*, *13*(1), 197–218. https://doi.org/10.5194/tc-13-197-2019

Yi, Y., Kimball, J. S., Chen, R. H., Moghaddam, M., Reichle, R. H., Mishra, U., et al. (2018). Characterizing permafrost active layer dynamics and sensitivity to landscape spatial heterogeneity in Alaska. *The Cryosphere*, *12*(1), 145–161. https://doi.org/10.5194/tc-12-145-2018

Yi, Y., Kimball, J. S., Rawlins, M. A., Moghaddam, M., & Euskirchen, E. S. (2015). The role of snow cover affecting boreal-arctic soil freeze-thaw and carbon dynamics. *Biogeosciences*, *12*(19), 5811–5829. https://doi.org/10.5194/bg-12-5811-2015

Zhang, T., Barry, R. G., Knowles, K., Heginbottom, J. A., & Brown, J. (2008). Statistics and characteristics of permafrost and ground-ice distribution in the Northern Hemisphere. *Polar Geography*, *31*(1–2), 47–68. https://doi.org/10.1080/10889370802175895

Zwieback, S., & Berg, A. A. (2019). Fine-scale SAR soil moisture estimation in the Subarctic tundra. *IEEE Transactions on Geoscience and Remote Sensing*, *57*(7), 4898–4912. https://doi.org/10.1109/TGRS.2019.2893908

Zwieback, S., Westermann, S., Langer, M., Boike, J., Marsh, P., & Berg, A. (2019). Improving permafrost modeling by assimilating remotely sensed soil moisture. *Water Resources Research*, *55*, 1814–1832. https://doi.org/10.1029/2018WR023247